Kantis: A new *Australopithecus* site on shoulders of the Rift Valley near Nairobi, Kenya

Emma Mbua[a, *], Soichiro Kusaka[b], Yutaka Kunimatsu[c], Denis Geraads[d], Yoshihiro Sawada[e], Francis H. Brown[f], Tetsuya Sakai[g], Jean-Renaud Boisserie[h], Mototaka Saneyoshi[i], Christine Omuombo[j], Samuel Muteti[k], Takafumi Hirata[l], Akira Hayashida[m], Hideki Iwano[n], Tohru Danhara[n], René Bobe[o], Brian Jicha[p], Masato Nakatsukasa[q, *]

[a]Department of Biological Sciences, Mount Kenya University, P.O Box 342-00100, Thika, Kenya

[b]Museum of Natural and Environmental History, Suruga, Shizuoka 422-8017, Japan

[c]Faculty of Business Administration, Ryukoku University, Fushimi, Kyoto 612-8577, Japan

[d]Sorbonne Universités - CR2P-MNHN, CNRS, UPMC-Paris 6 - CP 38, Muséum National d'Histoire Naturelle, 8 rue Buffon, F-75231 Paris Cedex 05, France;
Max Planck Institute for Evolutionary Anthropology, Department of Human Evolution Deutscher Platz 6 - D-04103 Leipzig - Germany

[e]402-1 Fukushima, Kurashiki 710-0048, Japan

[f]Department of Geology & Geophysics, University of Utah, Salt Lake City, UT, 84112, USA

[g]Department of Geoscience, Shimane University, Matsue 690-8504, Japan

[h]Institut de Paléoprimatologie, Paléontologie Humaine : Evolution et Paléoenvironnements (CNRS and Université de Poitiers), 6, rue Michel Brunet, 86073 Poitiers CEDX 9, France;
Centre Français des Etudes Ethiopiennes (CNRS and Ministère des Affaires Etrangères), P.O BOX 5554, ADDIS ABABA, ETHIOPIA

[i]Department of Biosphere-Geosphere Science, Okayama University of Science, Kita, Okayama 700-0005, Japan

[j]Department of Geology, University of Nairobi, 30197-001001, Nairobi, Kenya

[k]Department of Earth Sciences, National Museums of Kenya, P.O Box 40658-00100, Nairobi, Kenya

[l]Division of Earth and Planetary Sciences, Kyoto University, Sakyo, Kyoto 606-8502, Japan

[m]Department of Environmental Systems Science, Doshisha University, Kyotanabe, Kyoto 610-0321, Japan

[n]Kyoto Fission-Track Co., Ltd., Kita, Kyoto 603-8832, Japan

[o]Departamento de Antropología, Universidad de Chile, Santiago, Chile

[p]Department of Geology and Geophysics, University of Wisconsin-Madison, 1215 W. Dayton Street, Madison, WI 53706, USA

[q]Laboratory of Physical Anthropology, Kyoto University, Sakyo, Kyoto 606-8502, Japan

Corresponding authors

E-mail addresses: enmbua@gmail.com (E. Mbua);

nakatsuk@anthro.zool.kyoto-u.ac.jp (M. Nakatsukasa)

Keywords

Pliocene, Hominin, Fossils, Carbon stable isotope, Paleoenvironment

Abstract

Most Plio-Pleistocene sites in the Gregory Rift Valley that have yielded abundant fossil hominins lie on the Rift Valley floor. Here we report a new Pliocene site, Kantis, on the shoulder of the Gregory Rift Valley, which extends the geographical range of *Australopithecus afarensis* to the highlands of Kenya. This species, known from sites in Ethiopia, Tanzania, and possibly Kenya, is believed to be adapted to a wide spectrum of habitats, from open grassland to woodland. The Kantis fauna is generally similar to that reported from other contemporaneous *Au. afarensis* sites on the Rift Valley floor. However, its faunal composition and stable carbon isotopic data from dental enamel suggest a stronger C_4 environment than that present at those sites. Although the Gregory Rift Valley has been the focus of paleontologists' attention for many years, surveys of the Rift shoulder may provide new perspective on African Pliocene mammal and hominin evolution.

Introduction

Australopithecus afarensis is known from East African sites (Fig. 1a) dated between 3.7 Ma and 3.0 Ma (Brown et al., 2013) and regarded by some as ancestral to *Homo* and *Paranthropus*. The species has a wider distribution and evidently a greater tolerance toward relatively open and arid environments dominated by C_4 grasses than does the preceding *Au. anamensis* (Bedaso et al., 2013; Cerling et al., 2013). As reconstructed, paleohabitats of *Au. Afarensis* include a wide range of environments: for example, heterogeneous woodland at Laetoli (Kingston and Harrison, 2007; Harrison, 2011; Kingston et al., 2011), a mosaic of woodland and shrubland at Hadar (Reed, 2008), a mosaic of relatively open and mesic habitats at Dikika (Alemseged et al., 2005; Bedaso et al., 2013), and a bushland/woodland with floodplain grassland at Maka (White et al., 1993).

Here we report a new fossil locality, Kantis Fossil Site (KFS) on the outskirts of Nairobi, which is a Pliocene hominin site recognized on shoulder of the Gregory Rift Valley that has yielded fossils of *Au. Afarensis* and abundant remains of other vertebrates. The presence of *Au. afarensis* at KFS extends the geographical range of *Au. afarensis* to the highlands of Kenya and suggests that this species found suitable habitats in the Kenyan highlands. We provide geology and geochronological information for KFS, describe the morphology of hominin specimens, and present paleoenvironmental implications based on the faunal assemblage and stable carbon isotopic data of herbivorous mammalian dental enamel.

Methods

$^{40}Ar/^{39}Ar$ age determination and glass composition

Samples of the Kantis Basalt ("Ngongankaratite and tannbuschite" in Saggerson [1991]; see Geology section) and the Lower Kerichwa Tuff (Guth and Wood, 2011) were collected for $^{40}Ar/^{39}Ar$ age determination. Following gentle disaggregation in a mullite mortar, feldspar was concentrated from the Lower Kerichwa Tuff by repeated flotation in water, followed by magnetic separation on a Frantz Isodynamic separator. Individual grains were handpicked from the concentrate under a binocular microscope, avoiding those that were discolored or cloudy. The selected grains were then bathed in a 5% HF solution in an ultrasonic bath for 5 minutes to remove glass attached to the surface, and dried in an oven at 80 ºC. Basalt samples were crushed,

and fragments free of obvious phenocrysts were used for argon analysis. Samples were loaded into aluminum packets and placed into 1.5 cm diameter aluminum discs and co-irradiated with flux monitors for 4 hours at the Oregon State University TRIGA reactor in the Cadmium-Lined In-Core Irradiation Tube (CLICIT). Sanidine from the Fish Canyon Tuff (age 28.201 Ma; Kuiper et al., 2008) was used as the neutron fluence monitor. At the University of Wisconsin-Madison Rare Gas Geochronology Laboratory, samples and standards were fused using a 25 W CO_2 laser following the methods of Smith et al. (2008). Mass discrimination was assessed by analysis of $^{40}Ar/^{36}Ar$ air pipette aliquots throughout the analytical session and was calculated relative to a $^{40}Ar/^{36}Ar$ ratio of 295.5 (Steiper and Jager, 1977). Compositions of glass from the tuff samples obtained from the KFS were determined by electron microprobe using methods described in (Nash, 1992).

Zircon U-Pb age determination

Samples were taken from the trachytic tuff and the mudflow deposit in the fossiliferous bed for zircon U-Pb age determination. Zircons from two volcanic samples (tuff and volcanic mud flow deposit) were separated using standard magnetic and heavy liquid techniques, and then handpicked under a binocular microscope. Zircon yields were only 200 grains in 1.7 kg from the tuff sample (KY13011903B) and 1,200 grains in 0.3 kg from the mud flow deposit sample (KY13012102). The separated zircon grains were subhedral with rounded edges and were reddish to pale brown. Randomly selected zircon grains were mounted in a PFA Teflon sheet and polished with several diamond pastes. After chemical etching of spontaneous-fission tracks of ^{238}U on polished surfaces using an NaOH-KOH eutectic solution at 225°C for 38 hours, we selected zircon grains with relatively lower track density, assuming that they have younger fission-track age. Then, we polished zircon surfaces again prior to U-Pb dating analysis to prevent contamination from common Pb.

Zircon U-Pb dating was carried out using inductively coupled plasma mass spectrometry (ICP-MS) combined with an ArF Excimer laser-ablation sampling technique (e.g., Hirata and Nisbet, 1995; Iizuka and Hirata, 2004; Sakata et al., 2014) at the Laboratory for Planetary Science, Kyoto University. For laser ablation, a New Wave Research NWR193 laser ablation system (Fremont, CA 94538, USA) was used. Ablation pit sizes were 20 and 25 μm in diameter.

Other operational conditions are as follows: laser wave length = 193 nm, energy density = 2.2–2.3 J/cm^2, crater size = 20 μm or 25 μm, repetition rate = 8 Hz or 10 Hz, and carrier gas = He. The ICP-MS instrument used in this study was a Nu Instruments (Wrexham, UK) AttoM high resolution-magnetic sector field-ICPMS (Yokoyama et al., 2011). Operational conditions are: forward power = 1300 W, carrier gas = Ar, gas flow rate = 0.9 L min^{-1} (Ar and He gas), scanning mode = deflector jump, data acquisition protocol = batch, and integration time = 9 s. In order to determine the ^{238}U-^{206}Pb and ^{235}U-^{207}Pb ages, spot-analyses monitoring ^{202}Hg, ^{204}Pb (^{204}Hg), ^{206}Pb, ^{207}Pb, ^{232}Th, and ^{238}U were performed avoiding inclusions. The instrumental bias for the ^{206}Pb/^{238}U ratio was corrected by normalizing the ^{206}Pb/^{238}U ratio to 0.1792 using zircon standard 91500 (Wiedenbeck et al., 1995). The OD-3 zircon (ca. 33 Ma; Iwano et al., 2012, 2013) was used as a secondary standard to check the validity of results during each dating session.

Magnetostratigraphy

Samples for magnetic analysis were obtained from five horizons: the picrobasalt lava (KD4), three mud to very fine sand beds in the fossil-bearing sediment (KD1, KD2, and KD3), and the trachytic pyroclastic flow deposit (KD5). At each site, at least seven oriented samples were collected, and remanent magnetization of the volcanic samples was measured on a spinner magnetometer (Natsuhara SMD-88) and of the sediments using a cryogenic magnetometer (2G Enterprises 755R).

Morphological analysis

KFS hominin dental materials (two lower dp3s and one upper C) were metrically and morphologically compared with other Plio-Pleistocene hominin taxa, which include *Ardipithecus ramidus*, *Au. anamensis*, *Au. Afarensis*, and *Au. africanus*. For the ulna (KNM-RK 53525), comparison was made with three other *Au. afarensis* ulnae and ulnar specimens of later (Pleistocene) ages: Omo L40-19 (hominini *indet*.), OH 36 (*c.f. Paranthropus boisei*), and UW-88-62 (*Au. sediba*).

Stable isotopic analysis

One hundred sixteen samples were taken from fossilized mammal tooth enamel for carbon isotope analysis. The samples were removed from fractured enamel surfaces using a dental drill

with a tungsten carbide bit. Before taking the sample, adhered matrix or dentine was removed from each fracture surface. One to three mg of enamel were collected for each specimen. Carbon isotope ratios of these powdered samples were measured using an isotope ratio mass spectrometer equipped with a GasBench II preparation device (both from Thermo Fisher Scientific) at the Research Institute for Humanity and Nature. Small samples (ca. 0.5 mg) were weighed with Ag capsules and placed in sample vials. After flushing the vials with Helium gas, phosphoric acid (100%) was add to the samples and reacted for 24 hours at 25 °C. Then, carbon isotope ratios of evolved CO_2 were measured. Isotope ratios were normalized to a working standard that was calibrated against VPDB (Vienna PeeDee Belemnite). The analytical error was within 0.2 ‰. The carbon isotope ratios are expressed by delta-notation as follows: $\delta^{13}C$ (‰) = $(R_{sample}/R_{standard} - 1) \times 1000$, where R_{sample} and $R_{standard}$ is $^{13}C/^{12}C$ of sample and standard, respectively.

Isotopic ratios obtained were compared with those published from contemporaneous localities in East Africa (between 3.2 and 3.8 Ma): Koobi Fora (Lokochot Mb), East Turkana (Harris and Cerling, 2002; Harris et al., 2008); Lothagam (Kaiyumung Mb), West Turkana (Uno et al., 2011); Dikika (Sidi Hakoma, Denen Dora, Kada Hadar Mbs), Afar (Bedaso et al., 2013); Laetoli (Upper Laetolil Beds; Kingston, 2011; Kingston and Harrison, 2007). We consider that values < -8‰ indicate a pure C_3 diet and values >-2 ‰ a pure C_4 diet, following Uno et al. (2011).

Geology and geochronology

KFS is located on the margins of the eastern shoulder of the Gregory Rift on the outskirts of Nairobi (01.391 S, 36.724 E, altitude 1746 m; Fig. 1b). The surrounding area is a 1700–1800 m high plateau, that rises to the ~2450 m Ngong Hills west of the site. The site is named after a small seasonal river known as Kantis (“a fast flowing river” in the Maasai language) that drains the area and flows into the Mbagathi River, finally joining the Athi River. The site is tucked away between two private farms that are separated by the Kantis and was reported to E.M. by one of the farm owners in 2009. Although the presence of the bone bed was noted in the geological survey of Nairobi area (Saggerson, 1991), no systematic research had been conducted in this area prior to 2009. At the time of reporting the site, the farm owner noted that his family first saw fossilized bones on the dry Kantis valley in the mid 70’s, but at that time the importance

of the bones as a paleontological heritage was not appreciated. It was not until the media in Kenya initiated television programs related to paleontological research that local Kenyans began to acquire knowledge on the importance of fossils. As a result, KFS and several sites have since been identified through notifications from the local populace.

Around the site, widely distributed late Cenozoic volcanic rocks associated with minor sedimentary beds unconformably cover a metamorphic basement complex (Saggerson, 1991). Fossils at KFS derive from the base of a thin (~30 m), unnamed sequence of sedimentary and volcaniclastic rocks that are stratigraphically sandwiched between the picrobasalt lava, which was previously defined as the Ngong ankaratite and tannbuschite (Saggerson, 1991) and is defined as Kantis basalt in this paper, and the base of the Lower Kerichwa Tuff as mapped in Guth and Wood (2013).

Sedimentary strata at KFS

The sedimentary succession at the KFS consisting of four units (Level 1, Level 2, Kantis Tuff, and Level 3 beds) lies unconformably above apicrobasalt lava (Kantis Basalt; Fig. 2). The Kantis Basalt is massive and is highly porphyritic with phenocrysts of olivine and abundant clinopyroxene (cpx) in a groundmass of cpx, plagioclase, a small amount of biotite, and titaniferous magnetite. Most of the clinopyroxenes (phenocrysts and groundmass) are titaniferous and aluminous.

The Level 1–3 beds (up to 0.7 m) are similar to each other. They are moderately consolidated and consist of poorly sorted, matrix-supported lapilli tuff, containing angular trachyte pebbles and cobbles of lithic fragments (trachyte, pumice, tuff, and basalt; Fig. 3). The gray matrix is homogeneous and consists of trachytic material containing glass shards. The pebbles and cobbles do not show preferred grain fabric except at several locations of the Level 3 bed, where a backset structure (thrust-like structure; Nemec, 1990) was identified. The backset structure shows that the sediment was transported from the west, away from the rift center. The poor-sorting and matrix support suggest that they were deposited from high-viscosity sediment gravity flows (cf. Miall, 1996). The homogeneous tuffaceous matrix is suggestive of deposition by a volcanic mudflow (lahar; cf. Smith and Fritz, 1989) from the west.

The Kantis Tuff (up to 0.5 m thick) consists of two parts: gray mud layers with thin sand layers (each < 3 cm) and white coarse tuff layers (Fig. 3). The bed is broken into two large blocks in the fossil site and many small cracks are present within it, probably due to minor sliding induced by dragging of the tuff by the Level 3 sediments that were transported by a volcanic mud flow. The tuff bed in the area where the Level 2 bed is thinner than at other locations was probably deposited in a small depression suitable for a small pond. The sand layers are interpreted as being of flood origin from rivers. There are local large footprints in and on top of the tuff (Fig. 3). The latter are interpreted as underprints, which are formed by the impact of feet on layers below the surface on which the animal walked (Lockley, 1991). The presence of footprints and underprints implies that there were habitats for large animals (e.g., hippo, elephant, or rhino) near the locality.

The trachytic pyroclastic flow deposits are poorly sorted massive lapilli tuffs with welded parts, and contain fragments of pumice, trachyte, tuff, and obsidian in a fine- to medium-grained tuffaceous matrix.

Constituent materials of the Kantis Tuff, and the matrix of the lapilli tuffs in the mud flow (lahar) and in the pyroclastic flow deposits are the same: volcanic glass, fragments of anorthoclase, titaniferous and aluminous clinopyroxene, kaersutite, titaniferous magnetite, ilmenite, apatite, and zircon.

Compositions of glass from tuff and matrix of the volcanic mudflow (lahar) deposits are trachytic and are not compositionally distinguishable; mineral compositions are also very similar (Supplementary Online Material [SOM] Table S1). Thus, these pyroclastic materials were supplied from the same source. The matrix of the volcanic mudflow and the pyroclastic flow deposits has trachytic glass and the same mineral assemblage described above, but compositions of the glass and minerals are slightly different.

$^{40}Ar/^{39}Ar$ ages and glass compositions

Samples of the Kantis Basalt and the Lower Kerichwa Tuff were collected for $^{40}Ar/^{39}Ar$ age determination (SOM Table S2). Using the age of 28.201 Ma for the Fish Canyon Sanidine results in ages that are ~0.36% older than those used in recent compilations of ages at other sites, for

which an age of 28.10 Ma was employed (Brown et al., 2013). The lava from the stream underlying the fossil site yielded a $^{40}Ar/^{39}Ar$ weighted plateau age of 5.30 ± 0.02 Ma, and ages derived from normal and inverse isochron ages of 5.28 ± 0.05 Ma. A clast from the fossiliferous level that is petrographically very similar yielded indistinguishable results: a $^{40}Ar/^{39}Ar$ weighted plateau isochron age of 5.30 ± 0.01 Ma, and normal and inverse isochron ages of 5.28 ± 0.02 Ma. Errors stated are two standard deviations. An age of 2.77 ± 0.01 Ma was obtained on the Lower Kerichwa Tuff that lies ~25 m stratigraphically above the level of KFS. Poorly exposed strata between KFS and the Lower Kerichwa Tuff contain at least one very tuffaceous sandstone about 15 m above KFS.

Compositions of glass from the Kantis Tuff (K09-618B), a tuff in the overlying sequence (K09-619), and the Lower Kerichwa Tuff (K09-686) were determined by electron microprobe using methods described in Nash (1992). All are trachytes with rather high TiO_2 and CaO contents (SOM Table S3). Feldspar from the Lower Kerichwa Tuff has a composition $An_2Ab_{62}Or_{36}$, near the boundary between anorthoclase and soda-sanidine.

Zircon U-Pb ages

Samples for zircon U-Pb age determination were taken from the trachytic tuff and the mudflow (KY13011903B and KY13012102, respectively) in the fossiliferous Level 2 (SOM Table S4). Uncertainties of isotopic ratios and U-Pb ages are two standard deviations. The zircon grains were divided into four groups in terms of ages; Neoarchean (2629.9 ± 167.5 Ma), Neoproterozoic (600~700 Ma), Miocene (6~7 Ma), and Pliocene (3~4 Ma). The Neoarchean zircon was probably derived from basement rocks of the Tanzania Craton. The Neoproterozoic and Miocene zircon grains were most likely derived from the pan-African orogenic Mozambique belt and rift volcanic rocks, respectively.

Concordia diagrams for the youngest grain were plotted (Fig. 4) and the weighted mean $^{238}U–^{206}Pb$ ages for concordant data calculated using the Isoplot 3.6 program (Ludwig, 2008). Since the trends of discordant data for both samples are probably explained by common Pb contamination, the youngest grains were dealt with as single age population. The lower intercept ages of 3.3 ± 0.3 Ma for KY13011903B and 3.6 ± 0.2 Ma for KY13012102 were concordant with each other (Fig. 4). Calculated weighted mean ages using only the concordant ^{238}U-^{206}Pb are

3.4 ± 0.1 Ma (5 spots) for KY13011903B and 3.5 ± 0.2 Ma (8 spots) for KY13012102 and have higher precision (Fig. 4).

Magnetostratigraphy.

Samples for magnetic analysis were obtained from five horizons (Fig. 2): the picrobasaltlava (KD4), three mud to very fine sand beds in the fossil-bearing sediment (KD1, KD2, and KD3), and the trachytic pyroclastic flow deposit (KD5). Results of alternating field (AF) and thermal demagnetization showed that all samples had a characteristic component almost linearly decaying toward the origin between 10 to 70 mT, or 300 and 600 °C (Fig. 5a). The characteristic magnetic directions determined by principal component analysis are well concentrated near the geomagnetic field direction expected from the geocentric axial dipole model, with normal polarity except for one result from a block sample of the trachytic pyroclastic flow deposit (KD5) showing an anomalous direction (Declination = 278°; Inclination = 34°; Fig. 5b). We interpret that this fragment might have been rotated after cooling below the blocking temperature, and thus does not record the geomagnetic field at the time of deposition. Thus, the five horizons constitute a single normal polarity interval. Given the U-Pb ages of zircon (3.4 ± 0.1 Ma and 3.5 ± 0.2 Ma) and the normal polarity of the strata, the normal polarity zone can be assigned to the Gauss Normal Chron, and most likely to C2An.3n (3.330–3.596 Ma; Ogg, 2012). An age of ~3.45 Ma for the fossil bed is consistent with the age (2.77 ± 0.01 Ma) of feldspar from the Lower Kerichwa Tuff that lies about 25 m higher in the section. Table 1 summarizes the radiometric ages and magnetostratigraphy of the Kantis Basalt, fossiliferous beds, and Lower Kerichwa Tuff at KFS.

Hominin fossils

Over the last four years of research, 1,200 fossil elements have been collected from KFS. About 740 identifiable faunal specimens comprise 29 taxa including one hominin species (Table 2). The hominin dental sample consists of two left lower dp3s (KNM-RK 53000 andKNM-RK 53001) and a left upper canine (KNM-RK 57800) representing two juveniles and one adult.

KNM-RK 53001 is a left lower dp3 crown (Fig. 6a) that measures 8.7 mm mesiodistally and 6.9 mm buccolingually. The maximum oblique diameter is 9.3 mm. The occlusal outline of the

crown is an asymmetric ovoid, with the mesiobuccal portion protruding slightly. The buccal portion of its distal surface is broken, missing a small chip of enamel, but the lingual portion is preserved, and shows part of the distal interstitial wear facet. On the other hand, there is no mesial interstitial wear facet. The crown is moderately worn, exposing a small area of dentine on the protoconid, a tiny area of dentine on the metaconid, and a large area of dentine on the hypoconid. The protoconid is the largest and highest cusp.

The short preprotocristid runs down mesially to meet with the wide mesiolingual cingulum. This cingulum slightly runs down distolingually to end at the base of the metaconid. The mesial fovea defined by the preprotocristid, premetacristid, and mesiolingual marginal ridge faces mesiolingually. The lingual slope of the protoconid is inflated, restricting the mesial fovea. The metaconid is well-developed, but it is much smaller and slightly lower than the protoconid. The metaconid is positioned close to and distolingual to the protoconid. These two cusps are linked to each other by a short and oblique crest. The postprotocristid runs down distally to meet with the hypoconid. A very short groove runs down on the buccal surface from the base of the postprotocristid, and ends at a small but distinct pit. The hypoconid is the second largest cusp, but it is much lower than the protoconid and metaconid. The hypoconid is much more heavily worn than the other cusps. The entoconid is a small low cusp at the distolingual corner of the crown. It shows a weak wear facet. There may be another small cusplet on the distal margin of the crown between the entoconid and hypoconid, corresponding to the hypoconulid, though damage to the distal margin and occlusal wear have obscured the morphology of this area.

KNM-RK 53000 is another left lower dp3 crown (Fig. 6a). It measures 8.6 mm mesiodistally and 7.1 mm buccolingually. The maximum oblique diameter is 9.4 mm. The preservation is not as good as that of KNM-RK 53001, lacking a large chip of enamel from the distobuccal corner of the crown, but the tooth is less worn. Only the protoconid shows a small island of dentine exposure. The morphology of the preserved portion of the crown is similar to that of KNM-RK 53001. The mesial fovea is distinct and the metaconid is well-developed. The buccal groove separates the protoconid and the broken hypoconid. The entoconid is well differentiated.

Leakey et al. (1998) described a lower dp3 of *Au. anamensis* (KNM-KP 34725) from Kanapoi as intermediate between *Ardipithecus ramidus* and *Au. afarensis*. The *Au. anamensis* specimen is

more primitive than *Au. afarensis* in having a narrower crown, which lacks the buccal and lingual grooves so that the talonid is poorly differentiated (Leakey et al., 1998). On the other hand, the dp3s of *Au.afarensis* have a broader crown with a buccolingually expanded talonid, where the distal cusps are better differentiated, as well as a marked mesial fovea and well-developed metaconid (White et al., 1994). In these features, the Kantis lower dp3s are different from *Au. anamensis* and resemble those of *Au. afarensis* (Table 3, Fig. 6b). In the lower dp3 of *Au. africanus* (Taung Child), the talonid is more expanded buccolingually than in the Kantis specimens.

KNM-RK 57800 is a left upper canine with most of the root preserved (Fig. 6c). The crown is slightly worn at the apex and along the mesial and distal crests. A tiny area of dentine is exposed at the apex. The preserved buccal height measures 14.9 mm. The crown is as broad as it is long, as the root is bucally rotated. The mesial shoulder of the crown is positioned high. In buccal view, the mesial shoulder is located at about two thirds of the buccal crown height from the cervix. The distal shoulder is also high-positioned, being at half of the buccal crown height. The mesial and distal buccal grooves are obscure, being just faint depressions. The mesial and distal crests are thick and rounded. In lingual view, the mesial groove is deeply incised near the base of the mesial crest, but it does not extend much towards the apex. The lingual cingulum is restricted to the mesial and distal ends of the lingual aspect. There is a low basal swelling, from which a low and coarsely crenulated lingual pillar descends apically. The lingual surface distal to the lingual pillar is concave. The mesial style is poorly developed, while the distal style is better developed. Both of them, however, are unlike the prominently developed styles observed in the upper canine of *Au. anamensis* (KNM-KP 35893). The root is ca. 25 mm long with a number of cracks. Its cross section is a rounded triangle, with the mesiolingual, buccal, and distal surfaces. The mesiolingual and distal surfaces of the root are rather flat, though a wide shallow vertical groove is developed on the former. The buccal surface of the root is rounded, being convex mesiodistally and cervicoapically. The Kantis upper canine is distinguished from that of *Au. anamensis* in its high position of the mesial and distal shoulders, shorter mesial and distal crests, better developed lingual pillar, and much weaker development of the styles and buccal grooves (Fig. 6d). In these aspects, KNM-RK 57800 is more similar to canines of *Au. afarensis*.

Upper canine morphology of *Kenyanthropus platyops* is largely unknown. Although an upper canine in a maxillary fragment (KNM-WT 38343) has been discovered from Lomekwi in the Turkana Basin (Leakey et al., 2001), which is contemporaneous with Kantis, the Lomekwi canine is severely damaged. The distal half of the crown is broken off, and the remaining mesial portion is separated into buccal and lingual fragments by a wide mesiodistal crack in occlusal view. In their original description, Leakey et al. (2001) noted that this canine "seems low-crowned when compared with *A. afarensis* canines of similar size and degree of wear" without providing measurements. We think that estimation of crown height is difficult given the effects of occlusal wear and individual variation. What we can say is that the mesial shoulder of the crown of KNM-WT 38343 appears relatively high-positioned as in *Au. afarensis*. KNM-RK 57800 may be similar to the upper canine of *K. platyops,* but this limited "similarity" neither provides sufficient evidence to assign KNM-RK 57800 to *K. platyops*, nor eclipses the greater similarity to *Au. afarensis* canines.

KNM-RK 53525 is a proximal half portion of a left ulna of a large primate (Fig. 6e). The maximum length is 151 mm. The presence of the median trochlear keel, wide trochlear articular surface, low olecranon process, and anteroposteriorly flattened middle part of the shaft indicate that it is of a hominin, not of a large-sized cercopithecid (see below). Fusion of the olecranon epiphysis, development of muscles' attachment marks, and overall size suggest that this bone belongs to an adult male (Fig. 7). The proximal olecranon surface is widely eroded preserving only a small area (ca. 10 mm anteroposteriorly and 6 mm mediolaterally). This intact surface approximates the original, most proximal part of the olecranon. The medial and posterior surfaces of the olecranon are eroded. Borders of the articular surface of the trochlear notch are almost entirely eroded, except the lateral border and both tips of the olecranon and anconeal processes are lost.

Due to preservation, many standard osteometric measurements cannot be obtained on KNM-RK 53525. However, some measurements, including the minimally estimated ones, show that KNM-RK 53525 is most comparable to the male *Au. afarensis* ulna A.L. 438-1 from Hadar (Drapeau et al., 2005) in size (Table 4).

The trochlear notch surface is only gently keeled (= crested). Proximal and distal keeling angles (Drapeau et al., 2005) are 136° and 134°, respectively, and slightly more blunt than in other *Au. afarensis* individuals (SOM Table S4). Because of the damage on the anconeal and coronoid processes, olecranon orientation and trochlear notch orientation (Drapeau et al., 2005; Haile-Selassie et al., 2010) could not be evaluated. The radial notch measures >14.5 mm anteroposteriorly and >10.7 mm proximodistally (minimum estimates because of border erosion), and it is set at about 20° to the anteroposterior axis of the trochlear joint in top view.

Proximal diaphyseal morphology of KNM-RK 53525 closely resembles that of A.L. 438-1a (Figs. 6e and 7; also see Drapeau et al., 2005). The supinator crest, which starts from the posterior border of the radial notch, is strongly developed. The distal extension of the supinator crest becomes a blunt but distinct ridge that descends obliquely (posterodistally) to form the posterior ridge. The lateral surface delineated by this oblique/posterior ridge and the interosseous crest is wide and flat. Distal to the coronoid process, the anterior border appears as an acute ridge about 4 cm long, then becomes indistinct as a concave surface. Lateral to this acute ridge is a deep groove for the insertion of the brachialis muscle. The medial border of this area is a sharp and distinct ridge, which probably originally continued upward to the anteromedial border of the coronoid process. Posterior to this ridge, at about the level of the coronoid process, is a deep hollowed area for the origins of the flexor digitrum superficialis and pronator teres muscles. In A.L. 288-1, corresponding surface features can be defined. However, they differ in either shape or position. The supinator crest is more anteriorly positioned, less distinct, and much less salient laterally. The area delineated by the oblique/posterior ridge and interosseous crest is narrower and convex. The brachialis insertion is distinct but wider and shallower. The insertion area of the flexor digitrum superficialis and pronator teres muscles is merely a shallow concavity. We think that these differences are essentially related differences of body size and upper limb muscularity.

Anteroposterior curvature of the diaphysis of KNM-RK 53525 is moderately developed like that of A.L. 438-1a (Fig. 7). Although the entire bone is necessary for rigorous quantification of ulnar curvature, curvature of KNM-RK 53525 is more pronounced than in the corresponding portion of A.L. 288-1, UW-88-62, and Omo L40-19, and less so than in OH 36. Although whole shaft curvature of Omo L40-19 is nearly comparable to that of OH 36 (Drapeau et al., 2005), it is proportionally long and markedly curved in the middle-to-distal portion. Omo L40-19 is distinct

from all the other ulnae in the anteroposteriorly, extremely flattened proximal shaft (McHenry et al., 1976). In OH 36, the insertion area of the brachialis is more proximally positioned. The anterior ridge ascending to the beak of the coronoid is absent, although the medial ridge that delineates the brachialis insertion medially is present.

In summary, KNM-RK 53525 resembles A.L. 438-1a in both size and shape more than it does any other fossil hominin ulnae compared here. It is possible that this ulna and the upper canine KNM-RK 57800 derived from the same individual since they were excavated 30 cm apart on the same horizon (Level 2 bed). However, this possibility is not strongly supported given that two left lower dp3s have been recovered from the site.

Based on themorphological details described above, we assign the Kantis hominin to *Au. afarensis*. The age of the fossiliferous deposits at KFS (3.6–3.3 Ma) is consistent with this interpretation.

Faunal assemblage

Of the 1,200 fossil elements from KFS, 740 identifiable faunal specimens are assigned to 29 taxa (Table 2). Hippopotamids were dominant among large mammals ($N = 311$, 42% of the NISP). They are followed by bovids ($N = 183$, 25%), cercopithecids ($N = 73$, 13%), suids ($N = 67$, 9%), equids ($N = 39$, 5%), rhinocerotids ($N = 38$, 5%), giraffids ($N = 13$, 1.8%), elephantids ($N = 6$, 0.8%), carnivora ($N = 5$, 0.7%), and hominins ($N = 4$, 0.5%).

Hippopotamidae

The KFS hippopotamids belong to at least two different species. An unidentified species is represented by a single upper second molar that is distinguished from other Kantis material by its very large size. The rest of the collection is mostly attributable to the hippopotamid lineage that is found in the Turkana Basin during the Pliocene. This material displays features intermediate between the taxon found at Kanapoi and Allia Bay (aff. *Hippopotamus* cf. *protamphibius:* 4.2–4.1 Ma; Harris et al., 2003; Weston, 2003) and that found in the lower levels of the Omo Group formations (equivalent to Member B of the Shungura Formation: 3.4–2.9 Ma: aff. *Hippopotamus protamphibius turkanensis*; Gèze, 1985). The overall size of craniodental remains is comparable to that of the Kanapoi material (i.e., somewhat larger than the later Turkana material), displaying

a robust mandible, moderately expanded canine apophyses, and three well-developed incisors. However, the lower i3 is slightly more reduced compared to the i1 than is the case for the Kanapoi hippos. The cranium displays elevated orbits and sagittal crests that are more similar in elevation to those from lower Shungura or Koobi Fora than those at Kanapoi. The premolar row is somewhat more reduced than in the Kanapoi material, and upper P4s display morphologies reminiscent of the variability observed in later Turkana material. Therefore, for the time being, we keep the name aff. *Hippopotamus* cf. *protamphibius* for the material attributable to this lineage (see also Boisserie, 2005). The on-going revision of the Omo material, in addition to this new material from KFS, should lead to a more precise definition in the near future. Most of the postcranial elements are probably related to aff. *Hippopotamus* cf. *protamphibius*.

Suidae

Notochoerus euilus is abundant and is by far the most common suid species. Complete m3s have four pairs of pillars and a tricuspidate talonid; large upper canines much resemble those of specimens from the lower part of the Koobi Fora Formation. Neither *Nyanzachoerus kanamensis* nor *Kolpochoerus afarensis,* which are common in other contemporaneous Rift Valley localities together with *N. euilus* (Bishop, 2010), have been definitely recognized, although a smaller suid (*Kolpochoerus*?) is probably represented by tooth fragments.

Giraffidae

Sivatherium sp. is definitely identifiable by dental remains, none of which can be unambiguously referred to *Giraffa*.

Bovidae

The bovids include representatives of the tribes Alcelaphini, Hippotragini, Reduncini, Aepycerotini, Cephalophini, Bovini, Antilopini, and Tragelaphini. Alcelaphini, *Aepyceros* sp., and Bovini are dominant while Tragelaphini, Reduncini, and Cephalophini are quite rare. Even though sample size is small, the difference in faunal relative abundances is so marked that it is unlikely to change significantly with further collecting, compared to contemporary localities within the Rift Valley.

Two species of Alcelaphini are present: a large *Damaliscus* sp. and a diminutive indeterminate species. Large alcelaphin horn-cores (KNM-RK 51259, 53786, 57389) are more regularly and strongly spiraled than those of most alcelaphins, except some early Pleistocene *Damaliscus* (*D. agelaius* from Olduvai [Gentry and Gentry, 1978] and *D. strepsiceras* from Garba IV at Melka Kunturé [Geraads et al., 2004]). It also resembles *Parmularius pandatus* from Laetoli (Gentry, 1987, 2011) but, unlike KNM-RK 51259, *P. pandatus* has the long pedicel and posterior basal swelling typical of its genus. Therefore, we leave these specimens as cf. *Damaliscus* sp. nov. Dental remains indicate the presence of another, diminutive alcelaphin species (Alcelaphini gen. et sp. indet.), similar in size to an unidentified species from the Kada Hadar Member at Hadar (Geraads et al., 2012), or to *P. parvicornis* from the Upper Ndolanya beds at Laetoli (Gentry, 2011).

The only recognized hippotragin is close to *Oryx deturi* from Laetoli (Gentry, 2011) and Hadar (Geraads et al., 2012), characterized by the transverse compression of its horn-cores (instead of antero-posterior in modern forms). Several hippotragin teeth probably belong here as well. A single upper molar attests to the presence of Reduncini (*Kobus* sp.). Two horn-cores resemble those of the Laetoli impala (Aepycerotini) in their large size, transverse ridges, and curvature in lateral view, but are longer and almost straight in frontal view. They can be called *Aepyceros* aff. *dietrichi* (Gentry, 2011) but probably represent a new species, adding to the already great diversity of Plio-Pleistocene impalas.

Two upper molars have strong, rounded labial ribs but no mesostyle; these features best match those of the duikers (*Cephalophus* sp.: Cephalophini). A bovin metacarpal matches in size a metatarsal from Amado in the Woranso-Mille region (Geraads et al., 2009) and is tentatively attributed to *Ugandax* sp. A few teeth belong to an antilopin identifiable as *Gazella*. Tragelaphins are uncommon; one mandibular fragment definitely belongs to a large representative of this tribe, and a few teeth probably belong here as well.

Equidae

Equids are represented only by isolated teeth, preventing assignment to species. We keep the name *Hipparion* (s.l.) sp. for the KFS material, because the sole synapomorphy of

"*Eurygnathohippus*," presence of ectostylids (Eisenmann and Geraads, 2007), is absent in several KFS lower cheek teeth. There is no evidence of *Equus*.

Rhinocerotidae

Almost all rhino fossils are of *Ceratotherium mauritanicum*. Several specimens display a distinctly less derived tooth pattern than the modern "white" rhino (Geraads, 2005). A few teeth definitely belong to *Diceros*, but this genus is much less common.

Carnivora

A lower p4 (KNM-RK50508) with narrow tall cuspids displays the typical morphology of saber-toothed felids and is attributable to *Homotherium*. However, species identification will require revision of African members of this group. A left m2 was identified by L. Werdelin (pers. comm.) as *Enhydriodon*. An upper carnassial fragment belongs to *Crocuta.* The Herpestidae are represented by a P4 and a m1 that must be referred to two different genera.

Elephantidae

This family is represented by tooth fragments only.

Cercopithecidae

Most cercopithecid fossils belong to Papionini and they are attributable to a single taxon with large sexual dimorphism. The KFS papionin is distinct from *Theropithecus* and *Parapapio*, known from contemporaneous Turkana Basin sites (Jablonski and Leakey, 2008). The KFS papionin material is mainly comprised of isolated teeth, but it also includes a well-preserved cranium and a mandibular fragment. The KFS papionin lacks a deep fossa on the mandibular corpus, as well as the maxillary fossa and ridge in contrast to most papionins, and is similar in these features to *Parapapio* and *Pliopapio* (Jablonski and Leakey, 2008). The skull from KFS, however, shows a distinct anteorbital drop around the nasal region. This feature does not fit the facial morphology of *Parapapio*, where the nasal profile is relatively straight without a prominent anteorbital drop. The anteorbital drop is more or less developed in papionins other than *Parapapio*. Although molars of the Kantis papionin have cusps that are slightly compressed mesiodistally, they remain in a more primitive papionin condition compared to the specialized

molar morphology observed in *Theropitheus*, where the molar cusps are strongly pinched and usually higher, and the molar cingula are much better developed. The KFS papionin also differs from *Papio*, as it lacks a deep maxillary fossa, distinct maxillary ridges, as well as a deep mandibular fossa, and it has a relatively shorter muzzle. The KFS papionin is, therefore, left as Papionini indet.

Although represented by only a few isolated teeth and possibly an ulnar fragment, a large colobine is present, as is also the case in the primate communities of contemporaneous Turkana Basin sites and Laetoli (Jablonski and Leakey, 2008). Two upper molars (KNM-RK 55044 and KNM-RK 55512) are similar in size to the other KFS upper molars assigned to Papionini indet., but are distinguished from the latter in having higher and less inflated cusps, sharp occlusal crests, a much more reduced mesial lingual cleft, and lacking the parastyle and mesial buccal cleft. These specimens very likely belong to a large colobine species.

Biochronology

Biochronological conclusions from the large mammal fauna are not straightforward, probably because the KFS fauna, in the Kenyan highlands, does not easily correlate with lowland faunas; in particular, the bovid taxa that are potentially most useful, cf. *Damaliscus* and *Aepyceros*, do not look identical with previously named forms. Of course the absence of *Equus* implies an age greater than 2.3 Ma; the morphology of the *Oryx* horn-cores and the presence of *Notochoerus euilus* confirm this, but do not add precision. Thus, the large mammal fauna is in agreement with a ca. 3.4–3.5 Ma age, though it does not firmly support it.

Paleoecology

The dominance of *Oryx* and alcelaphins, together with the virtual absence of reduncins and tragelaphins among bovids, unambiguously point towards an open landscape, confirmed by the dominance of *Ceratotherium* among rhinos and a virtual absence of brachyodont suids and of the browsing *Giraffa*. The single specimen of *Cephalophus*, whose modern representatives are forest-dwellers, seems to go against this but, as noted in Gentry (2011), they may in fact have secondarily returned to close environments, and their close relative *Sylvicapra* is found in open landscapes.

In order to compare the faunal assemblage of KFS with those of other East African sites of similar ages more objectively, we performed two factor analyses. The first one (Fig. 8) uses the number of species in each locomotor and dietary category as columns and modern localities as rows (data from Reed, 1998), fossil sites being added a posteriori (illustrative). It shows that the point cloud of fossil sites covers only part of the modern one, implying that the fossil assemblages do not greatly differ from each other. In addition, the clouds only partly overlap, as if the fossil cloud was shifted in relation to the modern one (this issue is discussed in detail by Su and Harrison, 2007). This is probably because of taphonomic bias, but it forbids interpreting fossil assemblages similar to modern localities that are close on the graph (as was done, e.g., by DiMaggio et al., 2015). Among fossil sites, Kantis plots near Hadar and the Lower Lomekwi, and is farther from the Upper Laetolil Beds, but occupies a marginal position.

The second analysis (Fig. 9) was performed on fossil assemblages and a number of specimens in the various bovid tribes (the rare Cephalophini and *Brabovus* being illustrative). It clearly separates the Laetoli sites with high numbers of open-country antelopes from those with greater wood cover (lower right) or more grasslands (upper right). Again, Kantis occupies a marginal position with respect to contemporaneous Ethiopian and Northern Kenyan sites, but is closer to Laetoli because of its higher content of open-country forms.

Keeping in mind that these graphs should be interpreted with caution, because they represent only the plane of the first two axes, and because of taphonomic biases, we can conclude that the Kantis site samples a mammalian assemblage that, although generally similar to those of contemporaneous sites, differs from all of them, thus broadening the range of environments inhabited by *Au. afarensis*.

Stable carbon isotope

Stable carbon isotope ratios obtained from fossil mammal tooth enamel can be used to infer the proportion of consumption of C_3 and C_4 food resources (Cerling et al., 2003). To reconstruct the paleoenvironment at KFS, we sampled tooth enamel from seven mammalian families (Table 5; Fig. 10). The average $\delta^{13}C$ value of fossil tooth enamel from Kantis (-3.0 ± 2.9‰) is similar to values known from other *Au. afarensis* sites but significantly higher than that for mammals from Laetoli (Fig. 10; ANOVA: $F = 14.5$, $p < 0.01$). The average $\delta^{13}C$ value for the hippopotamid (aff.

Hippopotamus cf. *protamphibius*) is -2.2 ± 1.7‰ (N = 30), indicating a mixed C_3/C_4 to C_4-dominated diet. This value is significantly higher than that of hippopotamids from the Turkana Basin and Dikika (F = 6.3, $p < 0.01$), and quite comparable to values obtained for extant *Hippopotamus amphibius* (Boisserie et al., 2011). $\delta^{13}C$ values of bovids do not differ from those of Lothagam, Dikika, and Laetoli, although Dikika bovids have higher $\delta^{13}C$ values than Laetoli bovids (ANOVA: F = 7.9, $p < 0.01$). Of the 13 bovid specimens, seven are alcelaphins (SOM Table S5). The average $\delta^{13}C$ value of KFS alcelaphins is -4.3 ± 3.2‰ and compares well with the extant hartebeests (*Alcelaphus*spp.; Cerling et al., 2003) and with alcelaphins of Dikika and Laetoli (SOM Table S5). The $\delta^{13}C$ value of *Notochoeruseuilus* from this site is -0.9 ± 0.6‰ (N = 22), indicating C_4-dominated diets similar to those of *N. euilus*from other localities. Although the KFS average is slightly higher than the others, there is no statistical difference (ANOVA: F = 2.1, p = 0.08). The variation in $\delta^{13}C$ of the KFS sample is small compared to other localities (Bartlett-test: F = 7.5, $p < 0.01$). The value for the two rhinocerotid species (*Ceratotherium mauritanicum* [N = 25] and *Diceros* sp. [N = 1]) is -5.2 ± 1.2‰, showing a mixed C_3/C_4 signature like those in Laetoli and Dikika, while Lothagam (N = 3) shows a pure C_4 signal. Equids, giraffes, and elephantids also have $\delta^{13}C$ values similar to those of the respective taxa from other localities.

Discussion

Australopithecus afarensis was previously known from northern Ethiopia to northern Tanzania, a latitudinal spread from 11° N to 3° S (>1500 km). The presence of *Au.afarensis* in the Turkana basin of Kenya is contested (Kimbel 1988; Ward et al., 1999; Brown et al., 2001; Kimbel and Delezene, 2009; Wood and Leakey, 2011). The KFS hominin specimens are the first clear evidence of this species in Kenya. In addition, KFS is unique in Kenya in its location on the eastern shoulder of the Gregory Rift Valley, hence expanding the *Au. afarensis* range east of the Rift Valley.

In spite of differences at low taxonomic levels, the KFS fauna is generally similar to that known from contemporaneous sites within the Rift Valley. Dental enamel isotopic signals of the KFS mammals compare well to those documented in the same or related taxa from contemporaneous localities. This may suggest that similar environments (various mosaics of woodland, shrubland, and grassland) were present in this area 3.5 Ma.

However, KFS was likely more open compared to the localities within the Rift Valley. Unlike these localities, the KFS suid assemblage virtually lacks brachyodont species. The bovid samples are dominated by alcelaphins, *Aepyceros*, and *Oryx,* whereas tragelaphins and reduncins are rare. Browsing tragelaphins occur in high frequency in localities within the Rift Valley, such as Woranso-Mille in Ethiopia (Geraads et al., 2009), the Sidi Hakoma Member at Hadar (Geraads et al., 2012), and the Omo-Turkana basin in Kenya and Ethiopia (Gentry, 1985; Harris, 1991). In addition, hippopotamid dental enamel yielded relatively high $\delta^{13}C$ values. Considering the semiaquatic habits of the group, this suggests that vegetation surrounding water bodies at KFS was probably richer in C_4 plants than was the case at other sites of similar age. Hippopotamid remains are represented by several individuals of different biological age (including young specimens) and *Enhydriodon* sp. is present, which is strong evidence for perennial water bodies of metric to plurimetric depth at KFS. Taken together, these results suggest that a grassland-dominated (less wooded) environment, like the present Nairobi National Park habitats, was present in this area around 3.5 Ma. Cerling et al. (2011) suggested that woody cover was ~40–60% at fossil sites in the Omo-Turkana Basin and Awash Valley around 3.6 Ma, so a smaller fraction of woody cover may pertain at KFS.

Laetoli (Upper Laetoli Beds: ULB), which is located on the 1,700–1,800 m high Eyasi Plateau, is the only other Pliocene locality with a comparably high elevation, but it is located west of the Gregory Rift Valley. The KFS and Laetoli are markedly different in the paleoenvironment and fauna. The ULB are unique in having no evidence for an extensive body of water in the depositional area, although gullies and minor channels are relatively common (Ditchfield and Harrison, 2011). Streams and rivers were probably seasonal in the ULB and the landscape was much drier compared to the KFS. The mammalian faunal composition differs greatly between the KFS and ULB. A main difference is that no hippopotamid fossil has been collected from the ULB, where the dominant taxa are leporids, bovids, rodents, and giraffids (>6% of the NISP; Harrison, 2011). Notably, the relative abundance of cercopithecid fossils is much higher in the KFS than in the ULB (9.9% vs. 0.9% relative to the NISP or 39.9% vs. 2.6% relative to the number of identified bovid specimens). In the ULB, the semi-terrestrial *Parapapio ado* comprises two-thirds of the cercopithecid specimens and an arboreal colobin (cf. *Rhinocolobus* sp.) makes up most of the rest. Among the KFS cercopithecid remains, a new

unnamed papionin is predominant and colobinae fossils are very rare, suggesting that the KFS was not suitable for arboreal monkeys. Bovid assemblages of KFS and ULB differ less than those of other groups. Alcelaphini and Hippotragini are dominant bovids, whereas Reduncini and Tragelaphini are rare or absent (Gentry, 2011). The (near) absence of these tribes contrasts with other contemporaneous localities. On the other hand, Neotragini (overwhelmingly *Madoqua*, dik-diks), which is a prominent tribe along with Alcelaphini in the ULB bovid assemblage (Gentry, 2011; Su, 2011), are absent at KFS. Neotragines are also rare or absent in most East African Pliocene sites, but taphonomy and/or collecting procedures certainly partly explain this difference. In summary, the faunal characteristics of these highland localities are rather varied and suggest different environmental settings. Kantis was probably more mesic with less wood cover. The presence of *Au. afarensis* in both sites, therefore, endorses a greater tolerance of this hominin species for varying habitats. Perhaps this environment variability foreshadows the greater adaptability of early *Homo*, which probably appeared ca. 2.8 Ma. At that time, environments probably ranged from grassland (Upper Lomekwi, Fig. 9) to bush (Shungura C; Fig. 9) and open savannah (DiMaggio et al., 2015).

While the presence of *Au. afarensis* was well documented in Ethiopia and Tanzania, the evidence in Kenya was not clear. The occurrence of the species at KFS provides an intermediate point on the distribution of species between Ethiopia and Tanzania. The discovery of *Au. bahrelghazali* from the Chad Basin (Koro Toro) extended the habitat of *Australopithecus* westward from the Rift Valley (Fig. 1a; Brunet et al., 1995). Likewise, the presence of *Au. afarensis* at KFS indicates that the Pliocene hominins' range had spread eastward across the Rift margin and possibly further than that. For example, it cannot be precluded that the range of *Au. afarensis* expanded eastward from the present Nairobi area to the ancient Athi River channels and its plains. Although the Gregory Rift Valley has been the focus of paleoanthropologists' attention in East Africa for many years, surveys of the Rift shoulder may open a new perspective for African mammal and hominin evolution during the Pliocene.

Acknowledgments

We gratefully acknowledge financial support for this project from the Leakey Foundation, JSPS-NACOSTI, WennerGren Foundation, Paleontological Scientific Trust (PAST), the F. H.

Brown Rosenblatt Fund (University of Utah), and the National Museums of Kenya (NMK). Stable isotopic analysis was supported by Joint Research Grant for the Environmental Isotope Study of Research Institute for Humanity and Nature. We also owe our gratitude to the following people for advice on various aspects of this study: Bill Kimbel, Carol Ward, Stephen Frost, Lars Wedelin, Fred Spoor, Fredrick K. Manthi, H. Nakaya, NMK Field Crew at KFS, Stephen Kesuke, Francis LemayianKesuke, Simon Gatheru, and Dorothy Syanda.

References

Aiello, L.C., Wood, B., Key, C., Lewis, M., 1999. Morphological and taxonomic affinities of the Olduvai ulna (OH 36). Am. J. Phys.Anthropol. 109, 89–110.

Alemseged, Z., Wynn, J.G., Kimbel, W.H., Reed, D., Geraads, D., Bobe, R., 2005. A new hominin from the basal member of the Hadar Formation, Dikika, Ethiopia, and its geological context. J. Hum. Evol. 49, 499–514.

Bedaso, Z.K., Wynn, J.G., Alemseged, Z., Geraads, D., 2013. Dietary and paleoenvironmental reconstruction using stable isotopes of herbivore tooth enamel from middle Pliocene Dikika, Ethiopia: Implication for *Australopithecus afarensis* habitat and food resources. J. Hum. Evol. 64, 21–38.

Bishop, L.C., 2010. Suoidea. In: Werdelin, L., Sanders, W.J. (Eds.), Cenozoic Mammals of Africa. University of California Press, Berkeley, pp. 821–842.

Bobe, R., 2007.Patterns of abundance and diversity in late Cenozoic bovids from the Turkana and Hadar Basins, Kenya and Ethiopia.In: Bobe, R., Alemseged, Z., Behrensmeyer, K. (Eds.), Hominin environments in the East African Pliocene: an assessment of the faunal evidence. Springer, Dordrecht, pp. 129–157.

Boisserie, J.-R., 2005. The phylogeny and taxonomy of Hippopotamidae (Mammalia: Artiodactyla): a review based on morphology and cladistic analysis. Zool. J. Linn. Soc. 143, 1–26.

Boisserie, J.-R.,Zazzo, A., Merceron, G., Blondel, C., Vignaud, P., Likius, A., Mackaye, H.T., Brunet, M., 2005.Diets of modern and late Miocene hippopotamids: evidence from carbon isotope composition and micro-wear of tooth enamel. Palaeogeogr. Palaeoclimat. Palaeoecol. 221, 153–174.

Brown, B., Brown, F.H., Walker, A., 2001. New hominids from the Lake Turkana basin, Kenya. J. Hum. Evol. 41, 29–44.

Brown, F.H., McDougall, I., Gathogo, P.N., 2013. Age Ranges of *Australopithecus* Species, Kenya, Ethiopia, and Tanzania. In: Reed, K.E., Fleagle, J.G., Leakey, R.E. (Eds.), The Paleobiology of Australopithecus. Springer, Dordrecht, pp. 7–20.

Brunet, M., Beauvilain, A., Coppens, Y., Heintz, E., Moutaye, A.E., Pilbeam, D., 1995.The first australopithecine 2,500 kilometres west of the Rift Valley (Chad). Nature 378, 273–275.

Cerling, T.E., Harris, J.M., Passey, B.H., 2003. Diets of East African Bovidae based on stable isotope analysis. J. Mammal. 84, 456–470.

Cerling, T.E.,Wynn, J.G., Andanje, S.A., Bird, M.I., Korir, D.K., Levin, N.E., Mace, W., Macharia, A.N., Quade, J., Remien, C.H., 2011. Woody cover and hominin environments in the past 6 million years. Nature 476, 51–56.

Cerling, T.E., Manthi, F.K., Mbua, E., Leakey L.N., Leakey, M.G., Leakey, R.E., Brown, F.H., Grine, F.E., Hart, J.A., Kaleme, P., Roche, H., Uno, K.T., Wood, B.A., 2013. Stable isotope-based diet reconstructions of Turkana Basin hominins. Proc. Natl. Acad. Sci. USA 110, 10501–10506.

DiMaggio, E.N., Campisano, C.J., Rowan, J., Dupont-Nivet, G., Deino, A.L., Bibi, F., Lewis, M.E., Souron, A., Garello, D., Werdelin, L., Reed, K.E., Arrowsmith, J.R., 2015. Late Pliocene fossiliferous sedimentaryrecord and the environmental context ofearly *Homo* from Afar, Ethiopia. Science 347, 1355–1359.

Ditchfield, P., Harrison, T., 2011.Sedimentology, lithostratigraphy and depositional history of the Laetoli area. In: Harrison, T. (Ed.), Paleontology and Geology of Laetoli: Human Evolution in Context. Vol. 1: Geology, Geochronology, Paleoecology and Paleoenvironment. Springer, Dordrecht, pp. 47–76.

Drapeau, M.S.M., Ward, C.V., Kimbel, W.H., Johanson, D.C., Rak, Y., 2005. Associated cranial and forelimb remains attributed to *Australopithecus afarensis* from Hadar, Ethiopia. J. Hum. Evol. 48, 593–642.

Eisenmann, V., Geraads, D., 2007.The hipparion from the late Pliocene of Ahl al Oughlam, Morocco, and a revision of the relationships of Pliocene and Pleistocene African hipparions. Palaeont. Afr. 42, 51−98.

Gentry, A.W., 1985.The Bovidae of the Omo Group deposits, Ethiopia (French and American collections). In: Coppens, Y., Howell, F.C. (Eds.), Les faunes plio-pléistocènes de la basse vallée de l'Omo (Éthiopie). Tome 1 Périssodactyles, Artiodactyles (Bovidae). Éditions du CNRS, Paris, pp. 119–214.

Gentry, A.W., 1987.Pliocene Bovidae from Laetoli. In: Leakey, M.D., Harris, J.M. (Eds.), Laetoli, a Pliocene Site in Northern Tanzania. Clarendon Press, Oxford, pp. 378–408.

Gentry, A.W., 2011. Bovidae. In: Harrison, T., (Ed.), Paleontology and Geology of Laetoli: Human Evolution in Context. Vol. 2: Fossil hominids and the associated fauna. Springer, Dordrecht, pp. 363−465.

Gentry, A.W., Gentry, A, 1978. Fossil Bovidae (Mammalia) of Olduvai Gorge, Tanzania. Part I. Bull. Brit. Mus. (Nat. Hist.) Geol. 29, 289–446.

Gèze, R., 1985.Répartition paléoécologique et relations phylogénétiques des Hippopotamidae (Mammalia, Artiodactyla) du néogène d'Afrique Orientale. In: Fondation Singer-Polignac (Ed.), L'environnement des hominidés au Plio-Pléistocène. Masson, Paris, pp. 81−100.

Geraads, D., 2005. Pliocene Rhinocerotidae (Mammalia) from Hadar and Dikika (Lower Awash, Ethiopia), and a revision of the origin of modern African rhinos. J. Vert.Paleontol. 25, 451−461.

Geraads, D., Eisenmann, V., Petter, G., 2004. The Large Mammal Fauna of the Oldowayan sites of Melka-Kunturé, Ethiopia. In: Chavaillon, J., Piperno, M. (Eds.), Studies on the Early PalaeolithicSite of Melka Kunture, Ethiopia. IstitutoItaliano diPreistoria e Protostoria, Roma, pp. 169−192.

Geraads, D., Melillo, S., Haile-Selassie, Y., 2009. Middle Pliocene Bovidae from hominid-bearing sites in the Woranso-Mille area, Afar region, Ethiopia. Palaeont. Afr. 44, 59–70.

Geraads, D., Bobe, R., Reed, K., 2012. Pliocene Bovidae (Mammalia) from the Hadar Formation of Hadar and Ledi-Geraru, Lower Awash, Ethiopia. J. Vert.Paleontol. 32, 180−197.

Guth, A.,Wood, J.,2013. Geological Map of the Southern Kenya Rift. Digital Map and Chart Series DMCH016. Geological Society of America.

Haile-Selassie, Y., Latimer, B.M., Alene, M., Deino, A.L., Gibert, L., Melillo, S.M., Saylor, B.Z., Scott, G.R., Lovejoy, C.O., 2010.An early *Australopithecus afarensis*postcranium from Woranso-Mille, Ethiopia. Proc. Natl. Acad. Sci. USA 107, 12121−12126.

Harris, J.M., 1991. Family Bovidae. In: Harris, J.M., (Ed.), Koobi Fora Research Project, Vol. 3: The Fossil Ungulates: Geology, Fossil Artiodactyls and Palaeoenvironments. Clarendon Press, Oxford, pp. 139–320.

Harris, J.M., Cerling, T.E., 2002. Dietary adaptations of extant and Neogene African suids. J. Zool. Lond. 256, 45–54.

Harris, J.M., Leakey, M.G., Cerling, T.E., Winkler, A.J., 2003. Early Pliocene tetrapod remains from Kanapoi, Lake Turkana Basin, Kenya. In: Harris, J.M., Leakey, M.G. (Eds.), Geology and Vertebrate Paleontology of the Early Pliocene site of Kanapoi, Northern Kenya (Contributions in Science 498). Natural History Museum of Los Angeles County, Los Angeles, pp. 39–113.

Harris, J.M., Cerling, T.E., Leakey, M.G., Passey, B.H., 2008. Stable isotope ecology of fossil hippopotamids from the Lake Turkana Basin of East Africa. J. Zool. 275, 323–331.

Harrison, T., 2011. Laetoli revisited: renewed paleontological and geological investigations at localities on the Eyasi Plateau in Northern Tanzania. In: Harrison, T. (Ed.), Paleontology and Geology of Laetoli: Human Evolution in Context. Vol. 1: Geology, Geochronology, Paleoecology and Paleoenvironment. Springer, Dordrecht, pp. 1–15.

Hirata, T., Nesbitt, R.W., 1995. U-Pb isotope geochronology of zircons: Evaluation of the laser probe inductively coupled plasma-mass spectrometry technique. Geochim. Cosmochim. Acta 59, 2491–2500.

Iizuka, T., Hirata, T., 2004.Simultaneous determinations of U-Pb age and REE abundances for zircons using ArFexcimer laser-ICPMS. Geochem. J. 38, 229–241.

Iwano, H., Orihashi, Y., Danhara, T., Hirata, T., Ogasawara, M., 2012. Evaluation of fission-track and U-Pb double dating method for identical zircon grains- Using homogeneous zircon grains in Kawamoto Granodiorite in Shimane prefecture, Japan. J. Geol. Soc. Japan 118, 365–375.

Iwano, H., Orihashi, Y., Hirata, T., Ogasawara, M., Danhara, T., Horie, K., Hasebe, N., Sueoka, S., Tamura, A., Hayasaka, Y., Katsube, A., Ito, H., Tani, K., Kimura, K., Chang, Q., Kouchi, Y., Haruta, Y., Yamamoto, K., 2013. An inter-laboratory evaluation of OD-3 zircon for use as a secondary U–Pb dating standard. Island Arc 22, 382–394.

Jablonski, N.G., Leakey, M.G. (Eds.), 2008. Koobi Fora Research Project: Volume 6. The Fossil Monkeys. California Academy of Science, San Francisco.

Kimbel, W.H., 1988. Identification of a partial cranium of *Australopithecus afarensis* from the Koobi Fora Formation, Kenya. J. Hum. Evol. 17, 647–656.

Kimbel, W.H., Delezene, L.K.,2009. Lucy redux: A review of research on *Australopithecus afarensis.* Yearb. Phys. Anthropol. 140, 2–48.

Kingston, J.D., 2011. Stable isotopic analyses of Laetoli fossil herbivores. In: Harrison, T. (Ed.), Paleontology and Geology of Laetoli: Human Evolution in Context. Vol. 1: Geology, Geochronology, Paleoecology and Paleoenvironment. Springer, Dordrecht, pp. 293–328.

Kingston, J.D., Harrison, T., 2007. Isotopic dietary reconstructions of Pliocene herbivores at Laetoli: implications for early hominin paleoecology. Palaeogeogr. Palaeoclimatol. Palaeoecol. 243, 272–306.

Kuiper, K.F., Deino, A., Hilgen, F.J., Krijgsman, W., Renne, P.R., Wijbrans, J.R., 2008. Synchronizing rock clocks of Earth history. Science 320, 500–504.

Leakey, M.G., Feibel, C.S., McDougal, I. Ward, C., Walker, A., 1998. New specimens and confirmation of an early age for *Australopithecus anamensis*. Nature 393, 62–66.

Leakey, M.G., Spoor, F., Brown, F.H., Gathogo, P.N., Kiarie, C., Leakey, L.N., McDougall, I., 2001. New hominin genus from eastern Africa shows diverse middle Pliocene lineages. Nature 410, 433–440.

Lockley, M., 1991. Tracking Dinosaurs. Cambridge Univ. Press,.

Ludwig, K.R., 2008. User's Manual for Isoplot 3.6. A Geochronological Toolkit for Microsoft Excel. Berkeley Geochronology Center, Berkeley.

McHenry, H.M., Corruccini, R.S., Howell, F.C., 1976. Analysis of an early hominid ulna from the Omo Basin, Ethiopia. Am. J. Phys.Anthropol. 44, 295–304.

Miall, A.D., 1996. The Geology of Fluvial Deposits, Sedimentary Facies, Basin Analysis and Petroleum Geology. Springer, Berlin.

Moggi-Cecchi, J., Grine, F.E., Tobias, P.V., 2006. Early hominid dental remains from Members 4 and 5 of the Sterkfontein Formation (1966–1996 excavations): catalogue, individual associations, morphological descriptions and initial metrical analysis. J. Hum. Evol. 50, 239–328.

Nash, W.P., 1992. Analysis of oxygen with the electron microprobe: Applications to hydrated glass and minerals. Amer. Mineral. 77, 453–457.

Nemec, W., 1990.Aspects of sediment movement on steep delta slope. In: Cokella, A., Prior, D.B. (Eds.), Coarse-grained Deltas. Blackwell, Oxford, pp. 29–73.

Ogg, J.G., 2012.Geomagnetic polarity time scale. In: Gradstein, F.M., Ogg, J.G, Schmitz, M.D., Ogg, G.M. (Eds.), The Geologic Time Scale, Vol. 1. Elsevier, Boston, pp. 85–113.

Reed, K.E., 1998. Using large mammal communities to examine ecological and taxonomic structure and predict vegetation in extant and extinct assemblages. Paleobiology 24, 384–408.

Reed, K.E., 2008. Paleoecological patterns at the Hadar hominin site, Afar Regional State, Ethiopia. J. Hum. Evol. 54, 743–768.

Saggerson, E.P., 1991. Geological Map of the Nairobi Area.Mines and Geology Department, Nairobi.

Sakata, S., Hattori, K., Iwano, H., Yokoyama, T.D., Danhara, T., Hirata, T., 2014. Determination of U-Pb ages for young zircons using a laser ablation-ICP-mass spectrometry coupled with an ion detection attenuator device. Geostand. Geoanal. Res.38, 409–420.

Smith, G.A., Fritz, W.J., 1989. Volcanic influences on terrestrial sedimentation. Geology 17, 375–376.

Smith, M.E., Singer, B.S., Carroll, A.R., Fournelle, J.H., 2008. Precise dating of biotite in distal volcanic ash: Isolating subtle alteration using $^{40}Ar/^{39}Ar$ laser incremental heating and electron microprobe techniques. Amer. Mineral. 93, 784–795.

Steiger, R.H., Jäger, E., 1977. Subcommission on geochronology: convention on the use of decay constants in geo- and cosmochronology. Earth Planet. Sci. Lett. 36, 359–362.

Su, D.F., 2011. Large mammal evidence for the paleoenvironment of the Upper Laetoli and Upper Ndolanya beds of Laetoli, Tanzania.In: Harrison, T. (Ed.), Paleontology and Geology of Laetoli: Human Evolution in Context. Vol. 1: Geology, Geochronology, Paleoecology and Paleoenvironment. Springer, Dordrecht, pp. 381–392.

Su, D.F., Harrison, T., 2007. The paleoecology of the Upper Laetolil Beds at Laetoli.A reconsideration of the large mammal evidence.In: Bobe, R., Alemseged, Z., Behrensmeyer, K. (Eds), Hominin environments in the East African Pliocene: an assessment of the faunal evidence. Springer, Dordrecht, pp. 279–310.

Uno, K.T., Cerling, T.E., Harris, J.M., Kunimatsu, Y., Leakey, M.G., Nakatsukasa, M., Nakaya, H., 2011. Late Miocene to Pliocene carbon isotope record of differential diet change among east African herbivores. Proc. Natl. Acad. Sci. USA 108, 6509–6514.

Ward, C.V., Leakey, M.G., Brown, B., Brown, F., Harris, J., Walker, A., 1999. South Turkwel: a new Pliocene hominid site in Kenya. J. Hum. Evol.36, 69–95.

Ward, C.V., Plavcan, J.M.,Manthi, F.K.,2010. Anterior dental evolution in the *Australopithecus anamensis–afarensis*lineage. Phil. Trans. R. Soc. B 365, 3333–3344.

Weston, E., Boisserie, J.-R., 2010. Hippopotamidae. In: Werdelin, L., Sanders, W.J. (Eds.), Cenozoic Mammals of Africa. University of California Press, Berkeley, pp. 853–871.

Weston, E.M., 2003.Fossil Hippopotamidae from Lothagam. In: Leakey, M.G., Harris, J.M. (Eds.), Lothagam: The Dawn of Humanity in Eastern Africa. Columbia University Press, New York, pp 441–483.

White, T.D., Suwa, G., Hart, W.K., Walter, R.C., WoldeGabriel, G., Heinzelin, J. de, Clark, J.D., Asfaw, B., Vrba, E., 1993. New discoveries of *Australopithecus* at Maka, Ethiopia. Nature 366, 261–265.

White, T.D., Suwa, G., Asfaw, B.,1994. *Australopithecus ramidus*, a new species of early hominid from Aramis, Ethiopia. Nature 371, 306–312.

Wiedenbeck, M., Alle, P., Corfu, F., Griffin, W.L., Meier, M., Oberli, F., Von Quadt, A., Roddick, J.C., Spiegel, W., 1995. Three natural zircon standards for U-Th-Pb, Lu-Hf, trace element and REE analyses. Geostand. Newslett. 19, 1–23.

Wood, B., Leakey, M., 2011. The Omo-Turkana Basin fossil hominins and their contribution to our understanding of human evolution in Africa. Evol. Anthropol. 20, 264–292.

Yokoyama, T.D., Suzuki, T., Kon, Y., Hirata, T., 2011. Determinations of rare earth element abundance and U-Pb age of zircons using multispot laser ablation-inductively coupled plasma mass spectrometry. Analytical Chem. 83, 8892–8899.

Figure legends

Figure 1. Location maps of Kantis Fossil Site (KFS). a) The map showing *Australopithecus* sites mentioned in the text. b) Location of KFS in Kenya.

Figure 2. Columnar cross sections of the fossil site. Location of each section in the excavation site is indicated in the left upper inset. Strata at the KFS are divided into four beds (Level 1–3 and the Kantis Tuff) and are truncated by a terrace deposit. m = mud, s = sand, g = gravel.

Figure 3. Photographic explanation of sedimentary strata at the KFS. a) KFS main Trench. b) View of the outcrop. Note the poorly sorted gravel bed of Level 1 and the lenticular Kantis Tuff that tapers out at the left margin of the photograph. c) Close-up view of Level 1. Note that coarse gravels are scattered in fine sediments, showing matrix-supported nature. d) The Kantis Tuff bed. The dotted lines indicate traces of footprint. The local concave up stratal deformation (arrow) is interpreted as an underprint marked by a large animal.

Figure 4. Diagrams showing U-Pb age data determined for two samples KY13011903 (a) and KY13012102 (b) obtained from the fossil bed. The left panels are concordia diagrams using youngest grain data. The right panels show ^{238}U-^{206}Pb age distributions, excluding any discordant data. All age data were calculated and plotted using Isoplot 3.6 (Ludwig, 2008) and error bars are shown at the 2 s.d. level.

Figure 5. Results of paleomagnetic analysis. a) Representative results of alternative field (AF) and thermal demagnetization (Th) shown as Zijderveld vector diagrams. Open and closed circles show projections onto the vertical and horizontal planes, respectively. Numbers following the sampling location (KD1~5: see Fig. 2) denote specimen numbers. J_0 = magnetic intensity before demagnetization. b) Directions of characteristic remnant magnetizations from the five locations. Open and filled circles show equal-area projections in the upper and lower hemisphere, respectively.

Figure 6. Hominin fossil materials. a) KNM-RK 53001, a left dp3 (upper row), and KNM-RK 53000, a left dp3 (lower row). From left to right: occlusal (stereo), buccal, and lingual views. Scale = 5 mm b) Lower dp3s of *Australopithecus* spp. From left to right; *Au. afarensis* L.H. 2 (cast); *Au. afarensis* A.L. 33-43b (cast); *Au. Anamensis* KNM-KP 34725 (original); *Au. africanus*

Taung Child (cast). Except KNM-KP 34725, images were cropped from photographs of the mandibular right dental row and inverted for comparative purpose. Scale = 5 mm c) KNM-RK 57800, a left upper canine. From left to right: lingual, distal, labial, and mesial views. Scale = 1 cm d) Upper canine comparison. Left panel = lingual view, right panel = buccal view. Left to right: *Au. afarensis* L.H. 3 (left side, cast), KNM-RK 57800 (left side), *Au. anamensis* KNM-KP 35893 (right side). e) KNM-RK 53525, a proximal half portion of an adult left ulna. Eroded parts are shown with shading. Abbreviations: sp and arrow heads = supinator crest, ic = interosseous crest, br = insertion of the brachialis muscle, fd = origin of the flexor digitorum superficialis and pronator teres muscles. Scale = 5 cm

Figure 7. Comparative photographs of fossil hominin ulnae. Right specimens are reversed for comparison. Lateral (top) and anterior view (bottom). From left to right: KNM-RK 53525, *Au. afarensis* A. L. 438-1, *Au. afarensis* A.L. 288-1, *Au. sediba* UW-88-62, c.f. *Paranthropus boisei* OH 36, Hominini indet. L40-19. Scales = 1 cm

Figure 8. Correspondence analysis of the number of large mammal species (> 5 kg) in each dietary and locomotor category, in modern and fossil African assemblages, as in Reed (1998, 2008). Variables are: A = arboreal, AQ = aquatic, T = terrestrial, TA = terrestrial/arboreal, B = browser, C = meat, CB = meat/bone, CI = meat/invertebrates, F = fruits, FG = fresh grass, FI = fruit/insects, FL = fruits/leaves, G = grazers, I = insects, MF = mixed feeders, OM = omnivorous, R = roots/bulbs. Only modern localities are active and plotted with a symbol from 1 (forest) to 7 (desert), as in Reed (1998:App.1). All fossil localities are illustrative and plot within the lower right rectangle, enlarged at the upper left. Data for modern localities from Reed (1998). Category assignments may differ from previously published ones.

Figure 9. Correspondence analysis of the number of specimens in each bovid tribe, in East African fossil localities. Data from Su (2011:Table 19.6), Bobe et al. (2007), the Turkana database, Omo catalog, and Hadar catalog (by C. Campisano, identifications updated by DG). Open symbols are illustrative. Open circles are the individual localities of the Upper Laetolil Beds (only the total is used as an active variable).

Figure 10. Box and whisker plots of stable carbon isotope ratios ($\delta^{13}C$) obtained from fossilized mammal tooth enamel in the KFS and other *Au. afarensis* sites (for the data source, see Table 5). Taxon pooled data (top left) and data by family are shown.

Figure 1

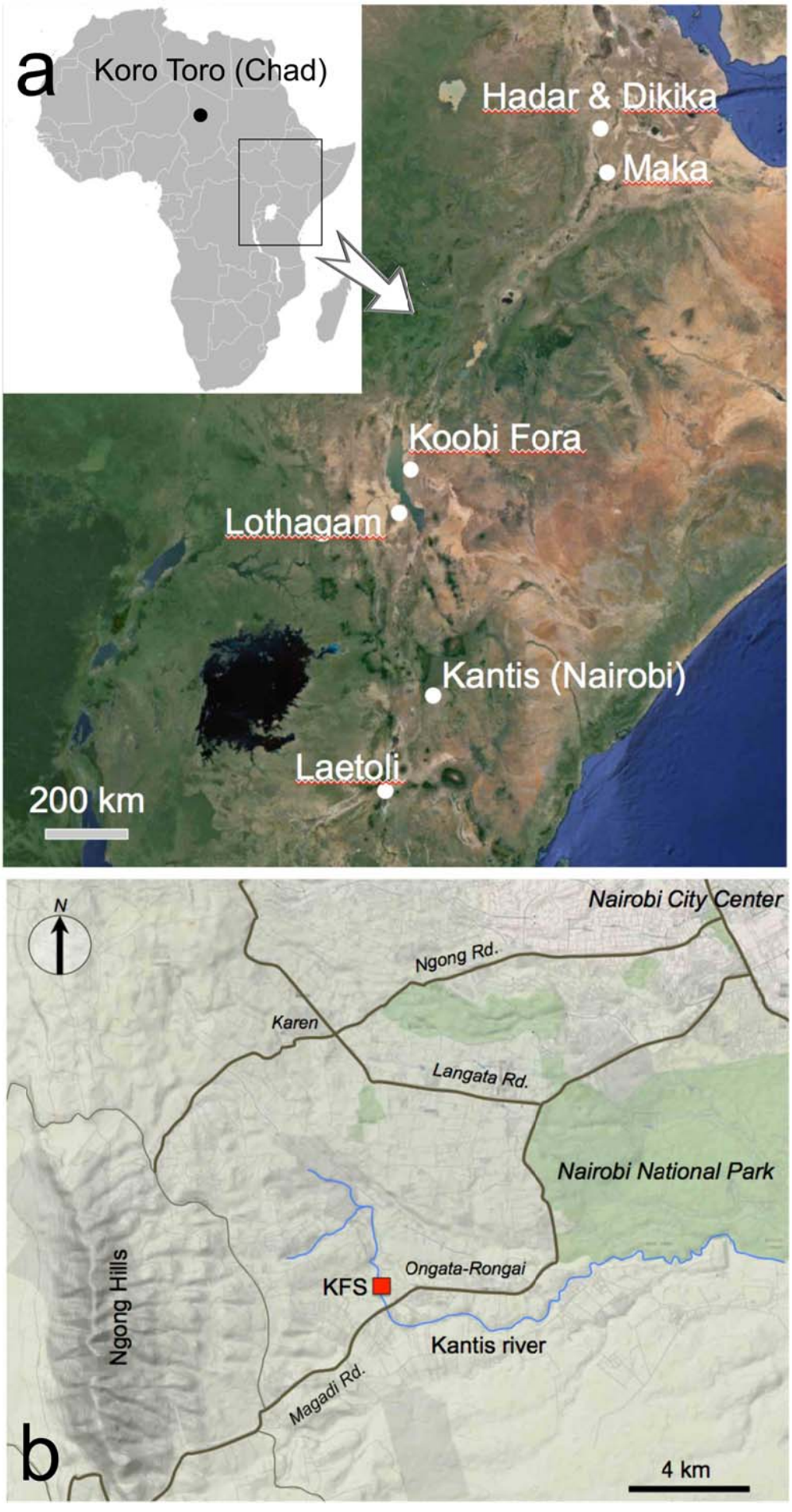
a
Koro Toro (Chad)
Hadar & Dikika
Maka
Koobi Fora
Lothagam
Kantis (Nairobi)
Laetoli
200 km
N
Nairobi City Center
Ngong Rd.
Karen
Langata Rd.
Nairobi National Park
Ongata-Rongai
KFS
Kantis river
Ngong Hills
Magadi Rd.
b
4 km

Figure 2

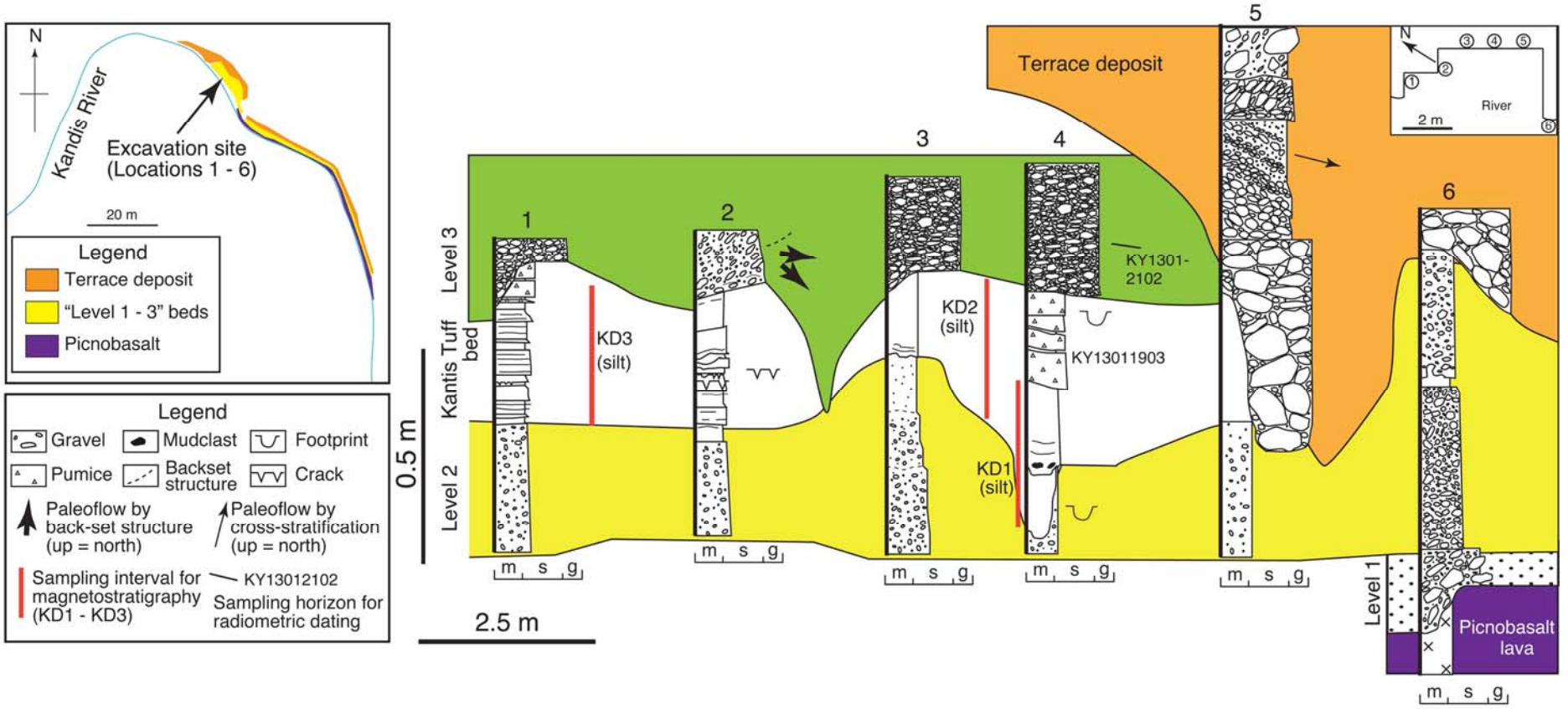
N
Kandis River
Excavation site
(Locations 1 - 6)
20 m
Legend
Terrace deposit
"Level 1 - 3" beds
Picnobasalt
Legend
Gravel
Mudclast
Footprint
Pumice
Backset structure
Crack
Paleoflow by back-set structure (up = north)
Paleoflow by cross-stratification (up = north)
Sampling interval for magnetostratigraphy (KD1 - KD3)
KY13012102
Sampling horizon for radiometric dating
Terrace deposit
Level 3
Kantis Tuff bed
Level 2
Level 1
0.5 m
2.5 m
KD3 (silt)
KD2 (silt)
KD1 (silt)
KY1301-2102
KY13011903
Picnobasalt lava
River
2 m
m s g

Figure 3


a
b
Terrace deposit
Level 3
Level 2
Level 1
Tuff bed
Picrobasalt
c
d
0.8 m
Tuff bed

Figure 4

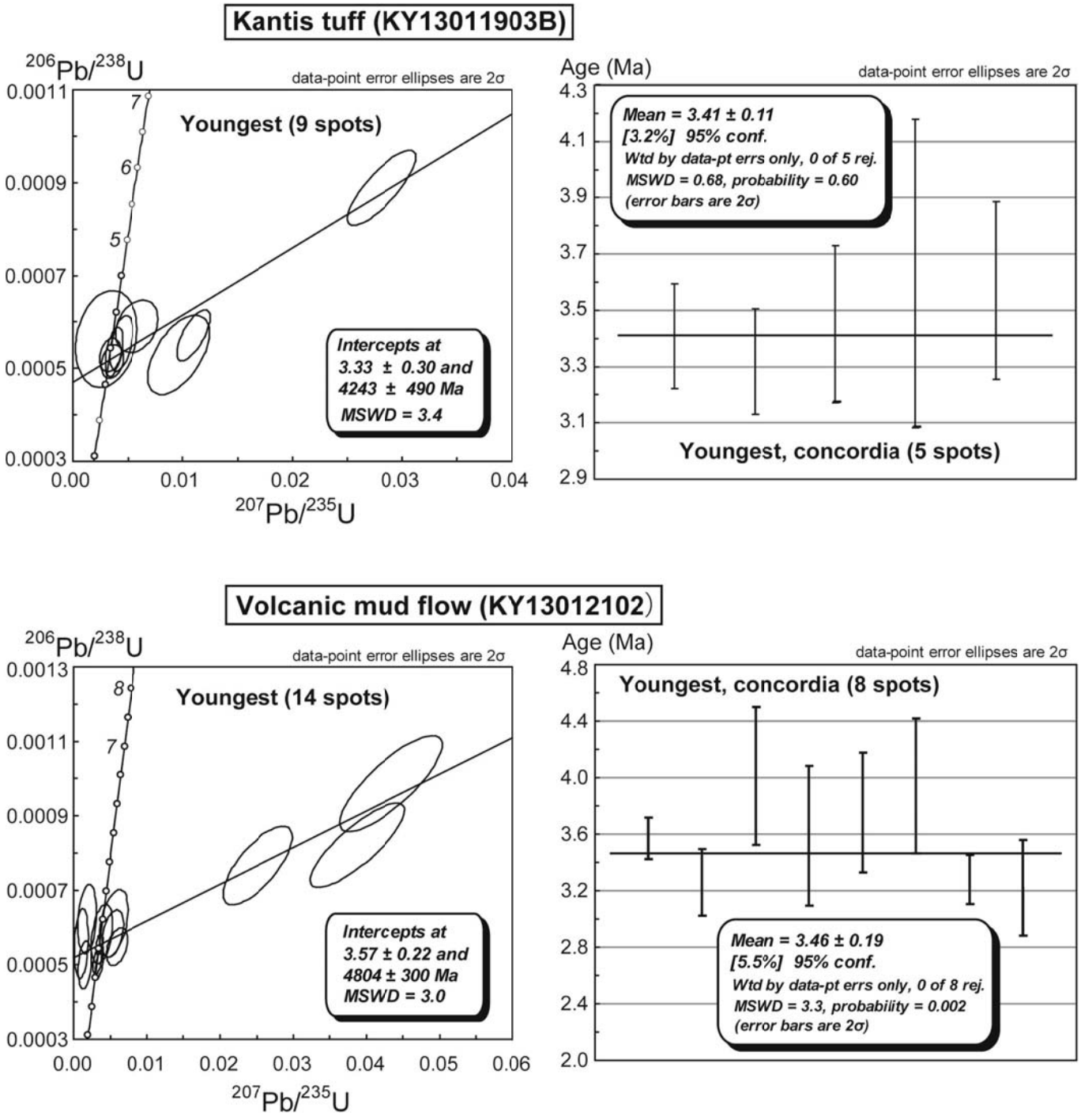
Kantis tuff (KY13011903B)
206Pb/238U
data-point error ellipses are 2σ
Youngest (9 spots)
Intercepts at
3.33 ± 0.30 and
4243 ± 490 Ma
MSWD = 3.4
207Pb/235U
Age (Ma)
Mean = 3.41 ± 0.11
[3.2%] 95% conf.
Wtd by data-pt errs only, 0 of 5 rej.
MSWD = 0.68, probability = 0.60
(error bars are 2σ)
Youngest, concordia (5 spots)
Volcanic mud flow (KY13012102)
Youngest (14 spots)
Intercepts at
3.57 ± 0.22 and
4804 ± 300 Ma
MSWD = 3.0
Youngest, concordia (8 spots)
Mean = 3.46 ± 0.19
[5.5%] 95% conf.
Wtd by data-pt errs only, 0 of 8 rej.
MSWD = 3.3, probability = 0.002
(error bars are 2σ)

Figure 5

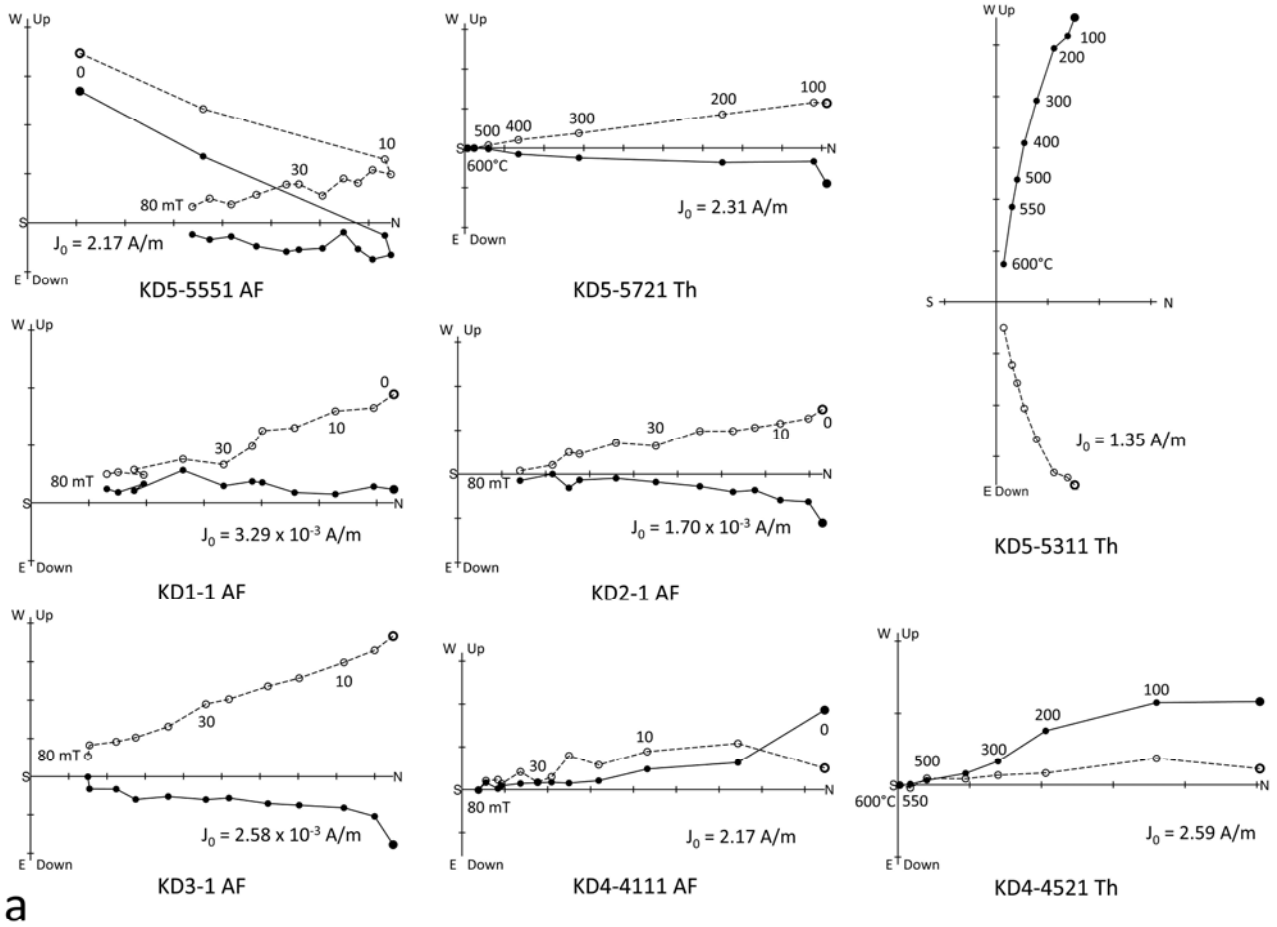
W Up
E Down
S
N
0
10
30
80 mT
J_0 = 2.17 A/m
KD5-5551 AF
500
400
300
200
100
600°C
J_0 = 2.31 A/m
KD5-5721 Th
550
J_0 = 1.35 A/m
KD5-5311 Th
J_0 = 3.29 x 10^{-3} A/m
KD1-1 AF
J_0 = 1.70 x 10^{-3} A/m
KD2-1 AF
J_0 = 2.58 x 10^{-3} A/m
KD3-1 AF
J_0 = 2.17 A/m
KD4-4111 AF
J_0 = 2.59 A/m
KD4-4521 Th
a

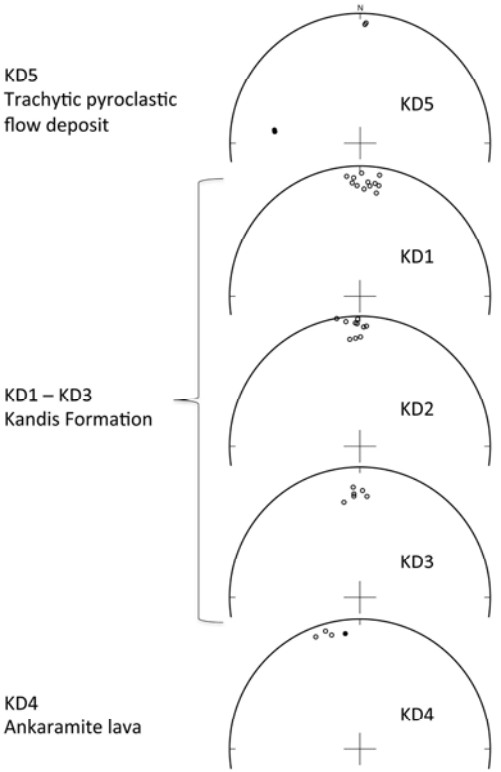
KD5
Trachytic pyroclastic
flow deposit
KD1 – KD3
Kandis Formation
KD4
Ankaramite lava
KD5
KD1
KD2
KD3
KD4
b

Figure 6

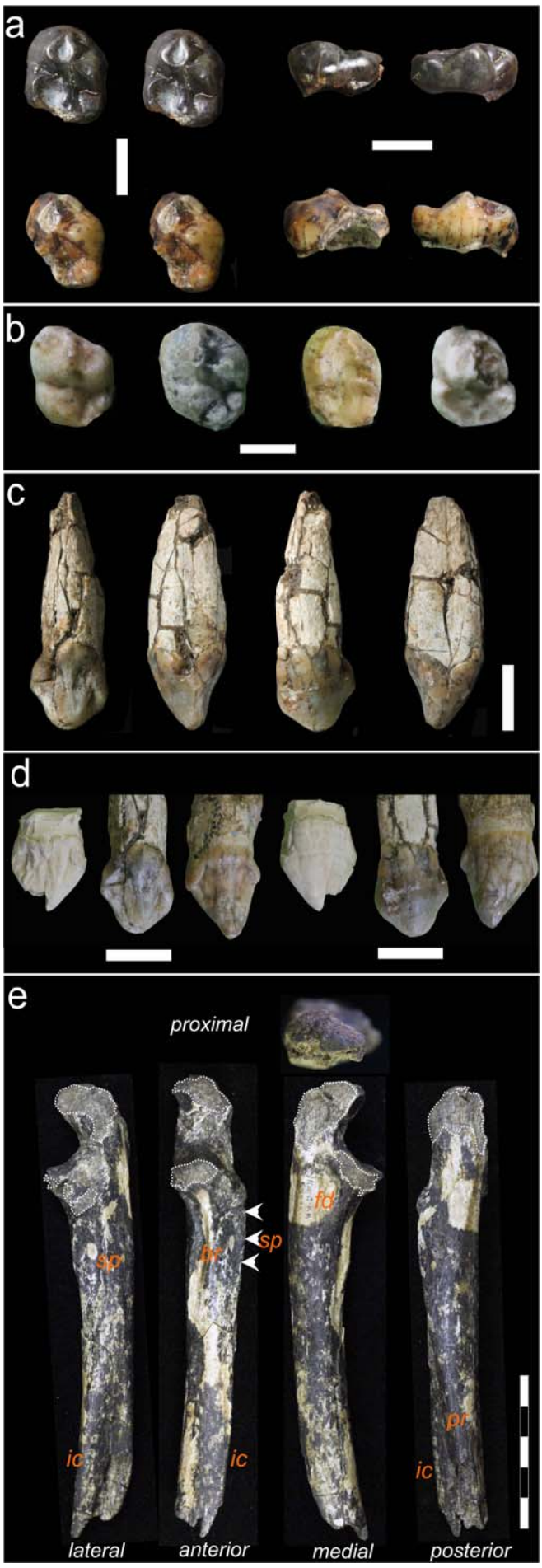
a
b
c
d
e
proximal
sp
hr
fd
sp
ic
ic
pr
ic
lateral
anterior
medial
posterior

Figure 7

Figure 8

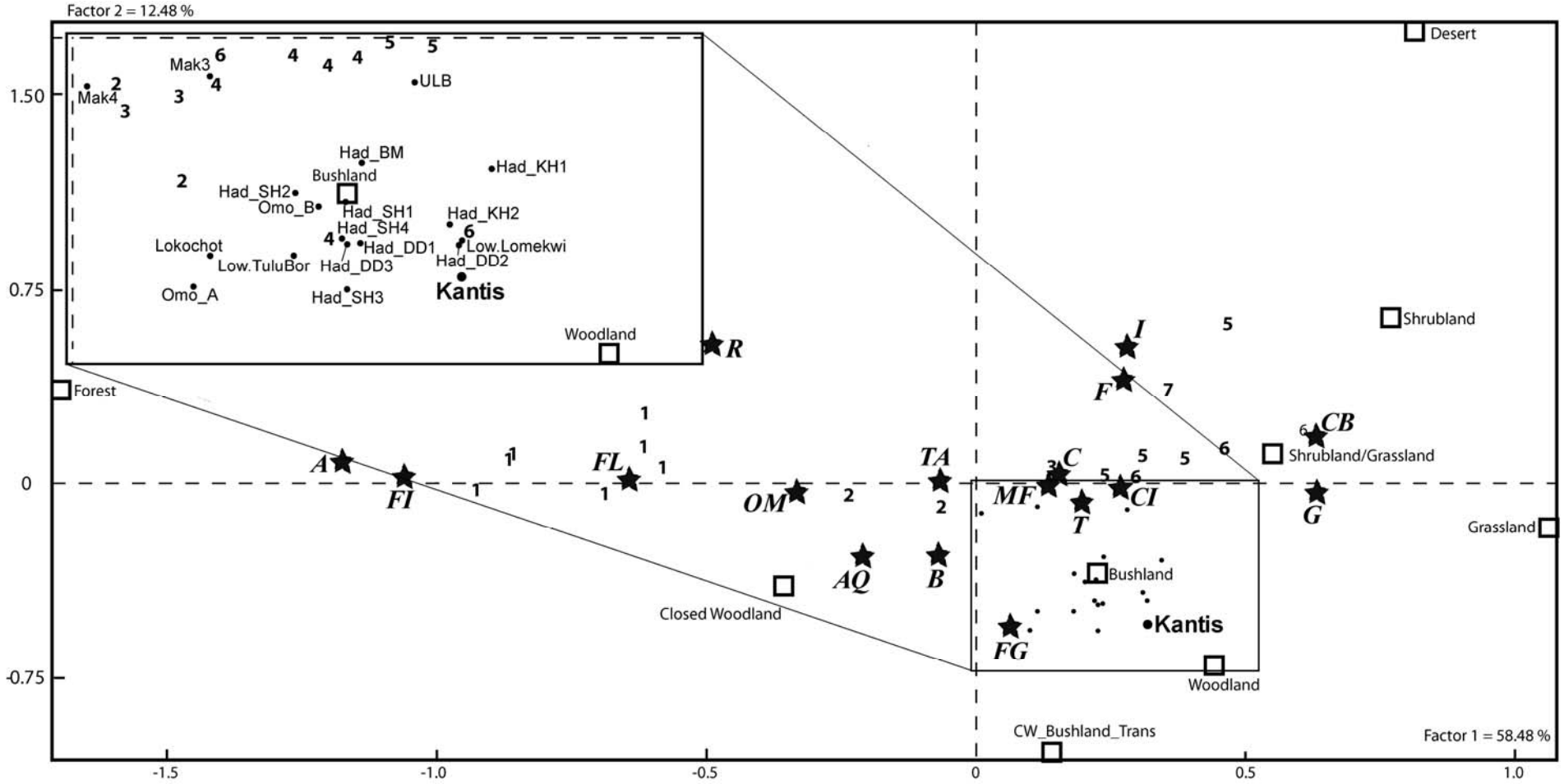
Factor 2 = 12.48 %
Factor 1 = 58.48 %
1.50
0.75
0
-0.75
-1.5
-1.0
-0.5
0
0.5
1.0
Mak3
Mak4
ULB
Had_BM
Had_KH1
Bushland
Had_SH2
Omo_B
Had_SH1
Had_KH2
Had_SH4
Lokochot
Had_DD1
Low.Lomekwi
Low.TuluBor
Had_DD3
Had_DD2
Omo_A
Had_SH3
Kantis
Woodland
Forest
Desert
Shrubland
Shrubland/Grassland
Grassland
Bushland
Closed Woodland
Woodland
CW_Bushland_Trans
R
I
F
CB
A
FI
FL
TA
C
MF
CI
T
G
OM
AQ
B
FG

Figure 9

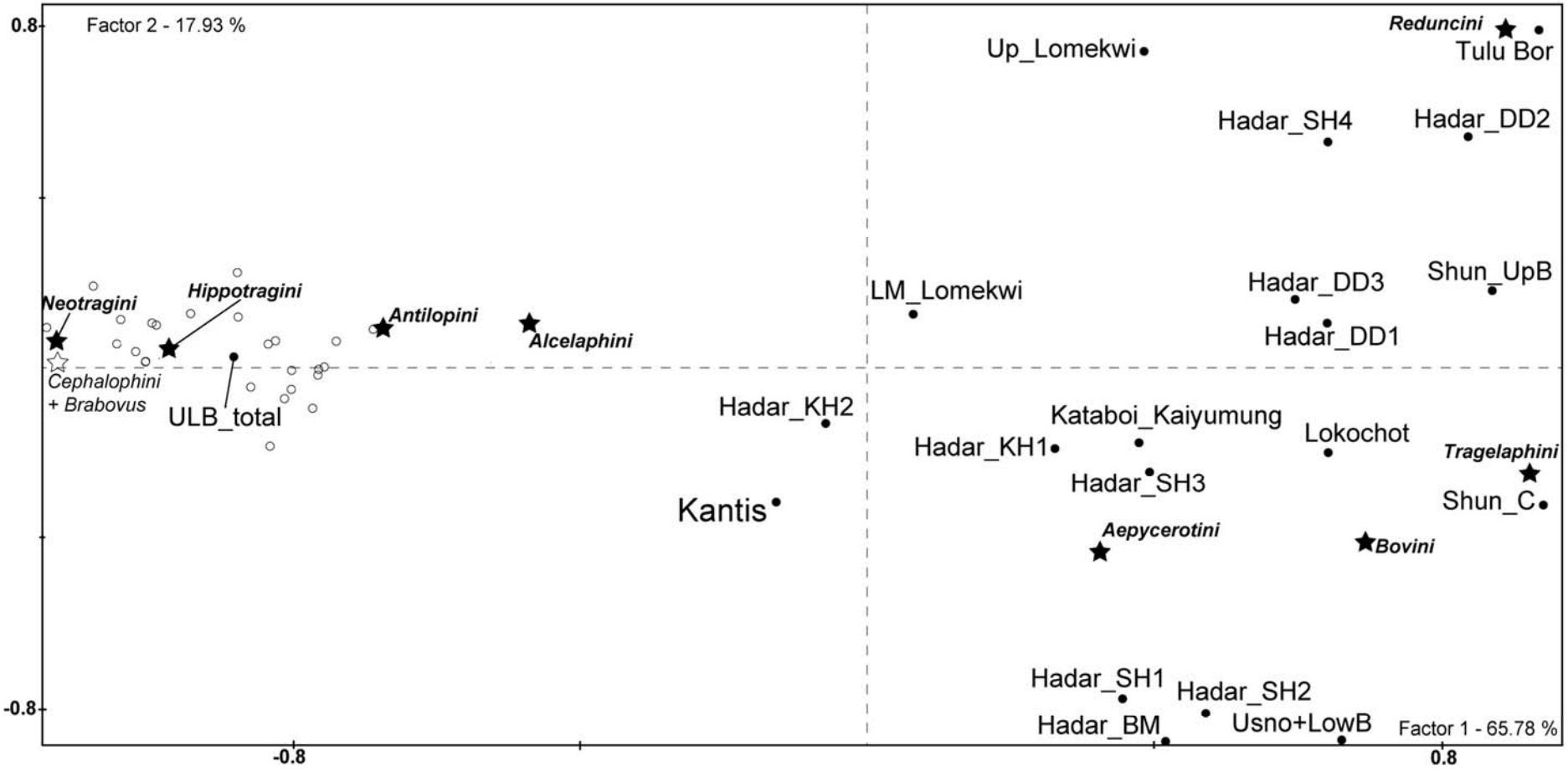
0.8
Factor 2 - 17.93 %
-0.8
-0.8
0.8
Factor 1 - 65.78 %
Reduncini
Tulu Bor
Up_Lomekwi
Hadar_SH4
Hadar_DD2
Shun_UpB
LM_Lomekwi
Hadar_DD3
Hadar_DD1
Neotragini
Hippotragini
Antilopini
Alcelaphini
Cephalophini
+ Brabovus
ULB_total
Hadar_KH2
Kataboi_Kaiyumung
Lokochot
Hadar_KH1
Tragelaphini
Hadar_SH3
Shun_C
Kantis
Aepycerotini
Bovini
Hadar_SH1
Hadar_SH2
Hadar_BM
Usno+LowB

Figure 10

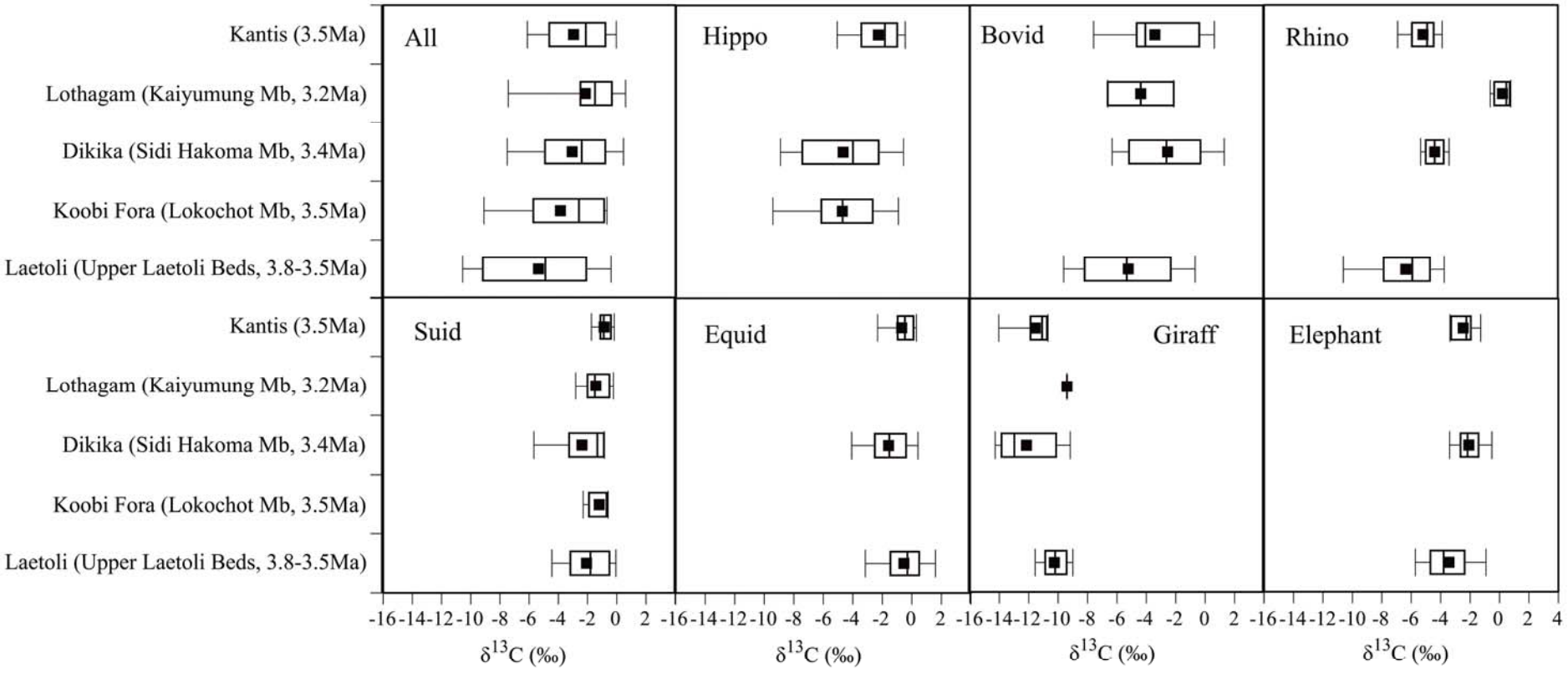
Kantis (3.5Ma)
Lothagam (Kaiyumung Mb, 3.2Ma)
Dikika (Sidi Hakoma Mb, 3.4Ma)
Koobi Fora (Lokochot Mb, 3.5Ma)
Laetoli (Upper Laetoli Beds, 3.8-3.5Ma)
All
Hippo
Bovid
Rhino
Suid
Equid
Giraff
Elephant
-16 -14 -12 -10 -8 -6 -4 -2 0 2 4
δ13C (‰)

Table 1. Summary of radiometric ages and magnetostratigraphy of the Kantis Basalt, fossiliferous beds, and Lower Kerichwa Tuff at KFS.

Stratigraphy	Radiometric age	Magnetic polarity	Geomagnetic polarity time scale[a]
Lower Kerichwa Tuff (trachyte pyroclastic flow deposits)	$^{40}Ar/^{39}Ar$ age of sanidine: 2.77 ± 0.01 Ma	Normal	C2An.1n: 2.581-3.032 Ma
Unconformity			
Kantis fossiliferous beds	Zircon U-Pb ages volcanic mud flow: 3.4 ± 0.1 Ma Kantis tuff: 3.5 ± 0.1 Ma	Normal	C2An.3n: 3.330-3.596Ma
Unconformity			
Kantis Basalt (picrobasalt lava flow)	$^{40}Ar/^{39}Ar$ ages of groundmass: 5.30 ± 0.02 Ma; 5.28 ± 0.05 Ma	Normal	

[a]Ogg (2012).

Table 2. KFS fauna list, with the number of identified specimens in each taxon (*N*), dietary preferences (Diet), and locomotor adaptations (Loc).

Order	Family	Tribe	Species	*N*	Diet[a]	Loc[b]
Primates						
	Hominidae	Hominini	*Australopithecus afarensis*	4	OM	T
	Cercopithecidae	Papionini	gen. et sp. indet.	66	FL	TA
		Colobini	gen. et sp. indet. (large)	7	FL	TA
Carnivora						
	Mustelidae	Enhydriodontini	*Enhydriodon* sp.	1	CI	AQ
	Felidae	Homotheriini	*Homotherium* sp	1	C	T
	Hyaenidae		*Crocuta sp.*	1	CB	T
	Herpestidae		Cf. *Ichneumia* sp.	1	CI	T
			Cf. *Mungos* sp.	1	CI	T
Proboscidea						
	Elephantidae		gen. et sp. indet	6	MF	T
Cetartiodactyla						
	Hippopotamidae		aff. *Hippo.* cf. *protamphibius*	310	FG	AQ
			Gen. et sp. indet.	1	FG	AQ
	Suidae			67		
			Notochoerus euilus	43	G	T
			Kolpochoerus sp.?	3	OM	T
	Giraffidae		*Sivatherium* sp.	13	B	T
	Bovidae			183		
		Tragelaphini	Gen. et sp. indet.	3	B	T
		Bovini	cf. *Ugandax* sp.	25	MF	T
		Alcelaphini		52		
			cf. *Damaliscus* sp. nov.	3	G	T
			gen. et sp. indet. (small)	4	G	T
		Hippotragini		12		
			Oryx cf. *deturi*	6	G	T
		Reduncini	*Kobus* sp.	1	FG	T
		Aepycerotini	*Aepyceros* aff. *dietrichi*	32	MF	T
		Cephalophini	*Cephalophus* sp.	2	B	T
		Antilopini	*Gazella* sp.	12	MF	T
Perissodactyla						
	Rhinocerotidae	Dicerotini	*Ceratotherium mauritanicum*	36	G	T
			Diceros sp.	2	B	T
	Equidae		*Hipparion* s.l. sp.	39	G	T
Rodentia						
	Thryonomyidae		*Thryonomys* sp.	1	FG	T
Aves			Gen. et sp. indet.			
Crocodylia						
	Crocodylidae		Gen. et. sp. indet.			

[a]Dietary preferences. OM=omnivores. FL=fruit and leaf eaters. CI=carnivores (meat and invertebrates). C=carnivores (meat only). CB=carnivores (meat and bone). MF=mixed feeders (browse and graze). FG=fresh-grass grazers. G=grazers. B=browsers.
[b]Locomotor adaptations. T=terrestrial. TA=terrestrial and arboreal. AQ=aquatic.

Table 3. Comparative dp3 and UC measurements and index: Mesiodistal (MD) and Buccolingual (BL) diameters.

dp3	MD (mm)	BL (mm)	BL/MD (%)	Source
Kantis				
KNM-RK 53001	8.7	6.9	79.3	
KNM-RK 53000	8.6	7.1	82.6	
Au. anamensis				
KNM-KP 34725	8.9	6.8	76.4	
Au. afarensis				White et al. (1994)
N	4	4	4	
Mean	9.2	7.9	86.8	
Range	8.5–9.6	7.6–8.4	81.9–94.1	
s.d.	0.5	0.4	5.4	
Au. africanus				White et al. (1994)
N	7	5		
Mean	8.8	7.6	86.4[a]	
Range	8.4–9.1	7.1–8.1	NA	
s.d.	0.2	0.4	NA	
P. robustus				White et al. (1994)
N	8	8		
Mean	10.1	8.3	82.2[a]	
Range	9–10.8	7.7–9.7	NA	
s.d.	0.5	0.6	NA	
Ar. ramidus				White et al. (1994)
ARA-VP-1/129	7.3	4.9	67.1	

UC	MD	BL	
Kantis			
KNM-RK 53800	11.5	11.6	
Au. anamensis			Ward et al. (2010)
N	8	7	
Mean	11.1	10.2	
Range	9.9–12.4	8.8–11.2	
s.d.	0.82	0.75	
Au. afarensis			Ward et al. (2010)

N	8	8	
Mean	9.8	10.7	
Range	8.9–11.6	9.3–12.5	
s.d.	0.84	1.00	
Au. africanus			Moggi-Cecchi et al. (2006)
N	13	13	
Mean	10.1	10.6	
Range	8.8–11.1	8.9–12.7	
s.d.	0.76	1.29	
Ar. ramidus			White et al. (1994)
ARA-VP-1/300	11.2	11.1	
ARA-VP-6/1	11.5	11.7	

[a]Calculated from averages of BL and MD.

Table 4. Measurements on hominin ulna.[a]

Specimen	Taxon	Age (Ma)	UTW	UPC	UCP	USM	UKN
KNM-RK 53525	*Au. afarensis*	3.5	11.5	16.5	(>29.5)	(>19.3)	136
A.L. 438-1	*Au. afarensis*	3.0	11.4	16.2	31.8	19.6	131
A.L. 288-1	*Au. afarensis*	3.4	12.3	12.4	22.5	15.2	132/130[c]
KSD-VP-1-1a	*Au. afarensis*	3.6	-	-	-	-	126
L40-19	hominini indet.[b]	2.3	17.3	20.8	33.4	23.9	121
OH 36	cf.*Paranthropus boisei*[2]	1.2	15.8	23.6	36.1	18.1	102
UW-88-62	*Au. sediba*	2.0	12.6	15.7	25.5	15.1	128

[a]Comparative metrics are adapted from Drapeau et al. (2005), except for KSD-VP-1-1a (from Haile-Selassie et al., 2010) and UW-88-62 (taken from cast at NMK).

Abbreviations: UTW = Mediolateral breadth of middle portion of the articular surface of the trochlear notch, UPC = Distance from posterior margin of ulna to the maximum depth of the keel of the trochlear notch, USM = Mediolateral breadth of the diaphysis immediately below radial notch, UKN = Keeling of trochlear notch measured as the angle between the articular surfaces of the trochlear notch on each side of the keel on the proximal part of the trochlear notch.

[b]Taxonomic assignment by Aiello et al. (1999).

[c]Right (A.L. 288-1n) and left ulnae (A.L. 288-1t).

Table 5. Isotopic analyses of enamel from fossil mammals at KFS, Lothagam (Kaiyumung Mb; 3.2 Ma), Laetoli (Upper Laetoli Beds; 3.8–3.5 Ma), Dikika (SidiHakoma Mb; 3.4 Ma), and Koobi Fora (Lokochot Mb; 3.5 Ma). For individual data, see SOM Table S6.

Taxon	Ste	*N*	Mean	S.D.	Reference
All					
	Kantis	127	-3.2	3.1	
	Lothagam	12	-2.2	3.0	Uno et al. (2011)
	Laetoli	239	-5.4	3.9	Kingston (2011)
	Dikika	131	-3.1	3.4	Bedaso et al. (2013)
	KoobiFora	13	-3.9	3.1	Harris and Cerling (2002), Harris et al. (2008)
Hippopotamidae					
	Kantis	30	-2.5	2.4	
	Dikika	11	-4.6	3.2	Bedaso et al. (2013)
	KoobiFora	10	-4.7	3.1	Harris et al. (2008)
Bovidae					
	Kantis	15	-3.3	3.5	
	Lothagam	2	-4.4	3.2	Uno et al. (2011)
	Laetoli	87	-5.2	3.5	Kingston (2011)
	Dikika	57	-2.5	2.9	Bedaso et al. (2013)
(Alcelaphini only)					
	Kantis	8	-1.1	2.5	
	Laetoli	33	-2.4	2.4	Kingston (2011)
	Dikika	20	-0.1	2.0	Bedaso et al. (2013)
Suidae					
	Kantis	24	-0.9	0.6	
	Lothagam	6	-1.4	1.0	Uno et al. (2011)
	Laetoli	36	-1.9	1.9	Kingston (2011)
	Dikika	9	-2.4	2.1	Bedaso et al. (2013)
	KoobiFora	3	-1.2	1.0	Harris and Cerling (2002)

Giraffidae					
	Kantis	6	-11.3	1.4	
	Lothagam	1	-9.4	-	Uno et al. (2011)
	Laetoli	47	-10.3	1.1	Kingston (2011)
	Dikika	8	-12.2	2.1	Bedaso et al. (2013)
Rhinocerotidae					
	Kantis	29	-5.3	1.7	
	Lothagam	3	0.2	0.7	Uno et al. (2011)
	Laetoli	30	-6.4	2.5	Kingston (2011)
	Dikika	4	-4.4	0.8	Bedaso et al. (2013)
Equidae					
	Kantis	17	-0.9	1.3	
	Laetoli	18	-1.0	1.9	Kingston (2011)
	Dikika	32	-1.6	1.5	Bedaso et al. (2013)
Elephantidae					
	Kantis	6	-2.9	1.4	
	Laetoli	21	-3.4	1.8	Kingston (2011)
	Dikika	10	-2.1	1.0	Bedaso et al. (2013)

SOM Table S1. Assemblage and chemical compositions of minerals (a) and chemical composition of the volcanic glass (b) in tuff and matrix of mud flow deposit, and pyroclastic flow deposit from KFS.

	KY13011903 Kantis Tuff	KY13012102 Volcanic mud flow	KY13012201 Lower Kerichwa Tuff pyroclastic flow	
(a)				
Feldspar				
Ca (An)	1.4～1.1	1.8～0.4	3.8～0.9	
Na (Ab)	61.6～61.5	66.3～60.9	72.8～66.2	
K (Or)	37.4～37.0	37.4～33.2	32.9～27.7	
Clinopyroxene (wt %)			(A)	(B) [1]
TiO_2	3.36～1.55	4.02～1.83	3.17～1.76	0.56～0.50
Al_2O_3	7.13～5.04	9.79～5.81	7.40～5.04	0.67～0.56
Na_2O	0.57～0.37	0.79～0.51	0.87～0.49	
(atomic ratio)				
Fe	12.2～9.8	15.4～10.3	13.7～11.3	25.7～23.3
Mg	41.9～37.5	40.7～33.6	39.4～37.5	36.5～32.0
Ca	50.3～48.0	51.5～48.6	50.1～48.0	42.4～39.6
mg-value	81.1～75.4	79.7～69.1	77.0～73.7	60.4～55.5
Amphibole (kaersutite)				
TiO_2 (wt %)	5.82～4.37	5.74～5.02	5.45～5.22	
mg-value	71.4～63.0	71.3～66.8	71.1～70.7	
Others	titaniferous magnetite Ilmenite Apatite Zircon	titaniferous magnetite ilmenite apatite zircon	titaniferous magnetite ilmenite apatite zircon	
(b)	mean (n=7)	s.d.	mean (n=10)	s.d.
SiO_2	65.04 [2]	0.37	65.41	0.26
TiO_2	0.82	0.06	0.81	0.06
Al_2O_3	14.55	0.39	14.63	0.17

FeO	5.96	0.12	5.87	0.14	6.61	0.10
MnO	0.31	0.05	0.27	0.04	0.33	0.05
MgO	0.58	0.03	0.54	0.04	0.50	0.03
CaO	0.88	0.05	0.88	0.04	0.84	0.05
Na_2O	6.47	0.14	6.26	0.12	7.43	0.29
K_2O	5.25	0.10	5.20	0.13	4.75	0.10
P_2O_5	0.14	0.01	0.14	0.04	0.12	0.03

[1] There are compositionally different groups of clinopyroxene, (A) and (B), in KY13012201.

[2] Wt %. Composition is volatile free.

SOM Table S2. $^{40}Ar/^{39}Ar$ data on sample K09-686, Lower Kerichwa Tuff (a), K11-771, Alkali basalt clast at KFS (b) and K09-620, Kantis Basalt at KFS (c).

(a)

Incremental Heating			$^{36}Ar(a)$	$^{37}Ar(ca)$	$^{38}Ar(cl)$	$^{39}Ar(k)$	$^{40}Ar(r)$	Age (Ma)	± 2σ	$^{40}Ar(r)$ (%)	$^{39}Ar(k)$ (%)	K/Ca	± 2σ
BG7332	35.0 %	✔	0.000643	0.011028	0.000000	0.620849	0.969441	2.77	± 0.01	83.60	15.34	24.208	± 0.489
BG7333	35.0 %	✔	0.000084	0.001131	0.000000	0.141066	0.220942	2.78	± 0.04	89.94	3.49	53.653	± 2.255
BG7335	35.0 %	✔	0.000359	0.002570	0.000000	0.183491	0.287813	2.78	± 0.03	73.07	4.53	30.699	± 0.640
BG7336	35.0 %	✔	0.001565	0.017680	0.000000	0.555518	0.865048	2.76	± 0.01	65.17	13.72	13.511	± 0.233
BG7338	35.0 %	✔	0.000189	0.005269	0.000111	0.298081	0.465829	2.77	± 0.02	89.30	7.36	24.327	± 0.592
BG7339	35.0 %	✔	0.000060	0.006709	0.000000	0.239465	0.373268	2.77	± 0.02	95.43	5.92	15.349	± 0.344
BG7341	35.0 %	✔	0.000126	0.008170	0.000000	0.190223	0.298774	2.79	± 0.03	88.89	4.70	10.011	± 0.251
BG7342	35.0 %	✔	0.000026	0.001942	0.000000	0.126134	0.198480	2.79	± 0.03	96.34	3.12	27.934	± 1.090
BG7344	35.0 %	✔	0.000121	0.005251	0.000074	0.227076	0.354517	2.77	± 0.03	90.83	5.61	18.595	± 0.385
BG7345	35.0 %	✔	0.000067	0.004056	0.000049	0.179543	0.282275	2.79	± 0.03	93.44	4.44	19.034	± 0.433
BG7347	35.0 %	✔	0.000206	0.003320	0.000012	0.212776	0.331333	2.76	± 0.02	84.48	5.26	27.557	± 0.775
BG7348	35.0 %	✔	0.000081	0.004233	0.000036	0.219706	0.344602	2.78	± 0.03	93.52	5.43	22.318	± 0.509
BG7350	35.0 %	✔	0.000139	0.004540	0.000000	0.166472	0.260039	2.77	± 0.03	86.35	4.11	15.767	± 0.465
BG7351	35.0 %	✔	0.000043	0.002117	0.000085	0.186268	0.289853	2.76	± 0.04	95.78	4.60	37.842	± 1.281
BG7353	35.0 %	✔	0.000053	0.001729	0.000038	0.093587	0.145517	2.76	± 0.06	90.32	2.31	23.277	± 1.043
BG7354	35.0 %	✔	0.000378	0.005052	0.000000	0.184707	0.288397	2.77	± 0.03	72.08	4.56	15.723	± 0.430
BG7356	35.0 %	✔	0.000612	0.004876	0.000000	0.222840	0.346979	2.76	± 0.04	65.74	5.51	19.650	± 0.499
		Σ	0.004752	0.089672	0.000406	4.047802	6.323106						

Information on Analysis		Results	$^{40}Ar(r)/^{39}Ar(k)$	± 2σ	Age (Ma)	± 2σ	MSWD	$^{39}Ar(k)$ (%,n)	K/Ca	± 2σ
K09-686		**Weighted Plateau**	1.5618	± 0.0032	2.77	± 0.01	0.51	100.00	16.864	± 2.891
Sanidine				± 0.20%		± 0.32%		17		
I10				External Error		± 0.11	2.12	Statistical T Ratio		
LAS				Analytical Error		± 0.01	1.0000	Error Magnification		
Project = UW91E		**Total Fusion Age**	1.5621	± 0.0035	2.77	± 0.01		17	0.544	± 0.004
Irradiation = UW91				± 0.22%		± 0.33%				
J = 0.0009706 ± 0.0000012				External Error		± 0.11				
FCs = 28.201 ± 0.023 Ma				Analytical Error		± 0.01				

(b)

Incremental Heating			^{36}Ar(a) [V]	^{37}Ar(ca) [V]	^{38}Ar(cl) [V]	^{39}Ar(k) [V]	^{40}Ar(r) [V]	Age (Ma)	± 2σ	^{40}Ar(r) (%)	^{39}Ar(k) (%)	K/Ca	± 2σ
CA0740	695 °C	✔	0.0005427	0.012080	0.0000825	0.0174915	0.0412475	5.38	± 0.58	20.46	0.40	0.623	± 0.057
CA0741	740 °C	✔	0.0012403	0.061809	0.0004306	0.0901344	0.2119148	5.37	± 0.15	36.64	2.07	0.627	± 0.039
CA0742	790 °C	✔	0.0004773	0.151715	0.0005788	0.2200905	0.5133893	5.33	± 0.05	78.45	5.06	0.624	± 0.036
CA0743	835 °C	✔	0.0005136	0.336931	0.0002987	0.5180713	1.2055675	5.31	± 0.02	88.82	11.90	0.661	± 0.038
CA0744	885 °C	✔	0.0004032	0.401806	0.0000614	0.5639796	1.3110802	5.31	± 0.03	91.67	12.96	0.604	± 0.034
CA0745	950 °C	✔	0.0006173	0.515683	0.0000000	0.5348873	1.2383532	5.29	± 0.03	87.16	12.29	0.446	± 0.025
CA0746	1020 °C	✔	0.0006740	0.536760	0.0000000	0.4009327	0.9275084	5.28	± 0.03	82.32	9.21	0.321	± 0.018
CA0747	1100 °C		0.0012317	1.408092	0.0003352	0.4342007	0.9832344	5.17	± 0.08	72.98	9.97	0.133	± 0.008
CA0748	1180 °C		0.0031310	8.196025	0.0010479	1.0040131	2.2234480	5.06	± 0.09	70.62	23.06	0.053	± 0.003
CA0749	1250 °C		0.0018989	7.130130	0.0005333	0.5692779	1.2876273	5.16	± 0.15	69.65	13.08	0.034	± 0.002
		Σ	0.0107301	18.751029	0.0033683	4.3530790	9.9433707						

Information on Analysis	Results	^{40}Ar(r)/ ^{39}Ar (k)	± 2σ	Age (Ma)	± 2σ	MSWD	^{39}Ar(k) (%,n)	K/Ca	± 2σ
Sample = K11-771	**Age Plateau**	2.32218	± 0.00574	5.30	± 0.01	0.91	53.88	0.474	± 0.113
Material = groundmass			± 0.25%		± 0.27%	48%	7		
Location = UW103C17			Minimal External Error		± 0.21	2.15	2σ Confidence Limit		
Analyst = Jicha, Brian			Analytical Error		± 0.01	1.0000	Error Magnification		
Project = UW103C									
Mass Discrimination Law = LIN	**Total Fusion Age**	2.28422	± 0.01349	5.22	± 0.03		10	0.100	± 0.003
Irradiation = UW103			± 0.59%		± 0.60%				
J = 0.00124920 ± 0.00000075			Minimal External Error		± 0.21				
FC = 28.201 ± 0.003 Ma			Analytical Error		± 0.03				

(C)

Incremental Heating			^{36}Ar(a) [V]	^{37}Ar(ca) [V]	^{38}Ar(cl) [V]	^{39}Ar(k) [V]	^{40}Ar(r) [V]	Age (Ma)	± 2σ	^{40}Ar(r) (%)	^{39}Ar(k) (%)	K/Ca	± 2σ
CA0809	695 °C	✔	0.0001037	0.038786	0.0000629	0.0574551	0.1342927	5.34	± 0.17	81.42	1.48	0.637	± 0.040

CA0810	740 °C	✔	0.0002352	0.131155	0.0000026	0.1837126	0.4283240	5.32	± 0.06	86.04	4.74	0.602	± 0.036
CA0811	800 °C	✔	0.0004640	0.365484	0.0000000	0.4897114	1.1352316	5.29	± 0.03	89.22	12.62	0.576	± 0.034
CA0812	845 °C	✔	0.0003823	0.351451	0.0000000	0.4483903	1.0390634	5.29	± 0.03	90.19	11.56	0.549	± 0.032
CA0813	895 °C	✔	0.0004672	0.396643	0.0000000	0.3730987	0.8659913	5.30	± 0.03	86.25	9.62	0.404	± 0.023
CA0814	960 °C	✔	0.0008026	0.550103	0.0001021	0.3741408	0.8692977	5.31	± 0.04	78.57	9.65	0.292	± 0.017
CA0815	1030 °C		0.0012691	1.047384	0.0000511	0.4177565	0.9436521	5.16	± 0.04	71.56	10.77	0.172	± 0.010
CA0816	1115 °C		0.0023476	3.904371	0.0008662	0.6480140	1.4641713	5.16	± 0.07	67.85	16.71	0.071	± 0.004
CA0817	1185 °C		0.0023841	7.697613	0.0007051	0.5651895	1.2657702	5.11	± 0.15	64.24	14.57	0.032	± 0.002
CA0818	1250 °C		0.0017630	4.992416	0.0003261	0.3214879	0.7285678	5.17	± 0.18	58.31	8.29	0.028	± 0.002
		Σ	0.0102188	19.475407	0.0021161	3.8789568	8.8743622						

Information on Analysis	Results	$^{40}Ar(r)/^{39}Ar(k)$	± 2σ	Age (Ma)	± 2σ	MSWD	$^{39}Ar(k)$ (%,n)	K/Ca	± 2σ
Sample = K09-620	**Age Plateau**		± 0.00663		± 0.02	0.29	49.67		
Material = groundmass	Overestimated Error	2.32018	± 0.29%	5.30	± 0.31%	92%	6	0.428	± 0.118
Location = UW103C21			Minimal External Error		± 0.21	2.26	2σ Confidence Limit		
Analyst = Jicha, Brian			Analytical Error		± 0.02	1.0000	Error Magnification		
Project = UW103C									
Mass Discrimination Law = LIN			± 0.01341		± 0.03				
Irradiation = UW103	**Total Fusion Age**	2.28782	± 0.59%	5.22	± 0.60%		10	0.086	± 0.003
J = 0.00124920 ± 0.00000075			Minimal External Error		± 0.21				
FC = 28.201 ± 0.003 Ma			Analytical Error		± 0.03				

SOM Table S3. Electron microprobe analyses of volcanic glass shards and feldspars from the section at KFS.

Sample	SiO_2	TiO_2	ZrO_2	Al_2O_3	Fe_2O_3	MnO	MgO	CaO	Na_2O	K_2O	F	Cl	Sum
Lower Kerichwa Tuff													
K09-686	62.1	0.78	0.10	14.7	5.84	0.30	0.52	0.73	6.60	6.07	0.25	0.19	98.2
K09-686	62.4	0.74	0.14	13.6	6.11	0.20	0.42	0.52	6.76	5.32	0.22	0.09	96.5
K09-686	63.0	0.82	0.25	14.0	5.89	0.22	0.36	0.55	6.81	5.37	0.15	0.12	97.6
K09-686	62.7	0.79	0.07	14.6	5.65	0.22	0.45	0.50	6.88	6.03	0.22	0.08	98.2
K09-686	62.9	0.75	0.14	14.4	5.84	0.27	0.42	0.55	6.98	5.56	0.15	0.10	98.1
K09-686	63.3	0.74	0.13	13.7	6.10	0.27	0.39	0.57	7.10	4.97	0.17	0.12	97.6
K09-686	62.3	0.74	0.05	15.0	5.56	0.18	0.46	0.69	7.16	5.20	0.28	0.07	97.6
K09-686	62.6	0.74	0.24	13.6	6.35	0.26	0.39	0.51	7.20	5.25	0.14	0.13	97.4
Average	**62.7**	**0.76**	**0.14**	**14.2**	**5.92**	**0.24**	**0.43**	**0.58**	**6.94**	**5.47**	**0.20**	**0.11**	**97.7**
s.d.	**0.4**	**0.03**	**0.07**	**0.6**	**0.26**	**0.04**	**0.05**	**0.08**	**0.21**	**0.39**	**0.05**	**0.04**	**0.6**
Tuffaceous sandstone in unnamed sequence between Kantis Phonolite and Lower Kerichwa Tuff													
K09-619	64.2	0.58	0.09	16.1	4.31	0.21	0.46	1.02	3.80	7.24	0.03	0.11	98.2
K09-619	65.3	0.60	0.09	16.1	4.43	0.23	0.41	1.01	4.47	6.33	0.05	0.12	99.2
K09-619	64.8	0.64	0.26	16.1	4.30	0.23	0.43	0.98	4.75	6.60	0.11	0.12	99.3
K09-619	65.6	0.65	0.02	16.3	4.39	0.21	0.40	1.08	4.86	5.49	0.12	0.10	99.2
K09-619	64.2	0.85	0.03	16.0	4.98	0.26	0.69	1.37	5.07	5.29	0.04	0.10	99.0
K09-619	65.9	0.51	0.11	16.0	4.12	0.22	0.36	0.86	5.47	5.91	0.08	0.16	99.8
K09-619	66.1	0.45	0.17	16.0	3.99	0.20	0.33	0.88	5.55	5.71	0.07	0.17	99.6
K09-619	65.2	0.74	0.22	16.2	4.51	0.27	0.51	1.17	5.79	5.31	0.01	0.10	100.1
K09-619	65.1	0.63	0.10	16.2	4.80	0.24	0.61	1.54	5.81	5.22	0.05	0.12	100.4
K09-619	66.5	0.59	0.17	16.2	4.17	0.23	0.33	0.84	5.84	5.35	0.15	0.15	100.5
K09-619	64.4	0.75	0.09	16.1	4.82	0.22	0.60	1.33	5.84	5.01	0.09	0.08	99.5
K09-619	66.0	0.50	0.09	16.1	4.14	0.24	0.32	0.83	5.87	5.45	0.07	0.17	99.8
K09-619	65.8	0.62	0.15	16.2	4.32	0.18	0.39	0.93	5.90	5.42	0.10	0.12	100.1
K09-619	66.0	0.51	0.21	16.1	4.28	0.26	0.32	0.92	5.92	5.35	0.05	0.13	100.0
K09-619	65.6	0.65	0.11	16.0	4.16	0.23	0.41	0.97	5.95	5.63	0.07	0.13	99.9
K09-619	66.0	0.51	0.24	15.8	4.23	0.20	0.37	0.85	5.96	5.21	0.11	0.17	99.7
K09-619	65.8	0.63	0.25	16.1	4.17	0.22	0.32	0.88	6.03	5.44	0.03	0.15	100.0
K09-619	63.1	1.12	0.12	16.2	5.29	0.24	0.89	1.68	6.15	5.02	0.06	0.07	100.1
K09-619	65.7	0.62	0.19	16.1	4.42	0.22	0.43	0.89	6.26	5.27	0.12	0.14	100.3
Average	**65.3**	**0.64**	**0.14**	**16.1**	**4.41**	**0.23**	**0.45**	**1.05**	**5.54**	**5.59**	**0.08**	**0.13**	**99.7**
s.d.	**0.9**	**0.15**	**0.07**	**0.1**	**0.33**	**0.02**	**0.15**	**0.25**	**0.65**	**0.57**	**0.04**	**0.03**	**0.6**
Kantis Tuff													
K09-618B	61.2	1.00	0.08	14.5	6.47	0.30	0.59	0.92	5.25	5.31	0.23	0.07	95.9
K09-618B	63.1	0.90	0.11	14.3	6.60	0.29	0.51	0.88	5.26	5.16	0.26	0.08	97.5
K09-618B	63.6	0.95	0.05	14.1	6.64	0.31	0.54	0.85	4.95	5.05	0.30	0.08	97.4
K09-618B	63.1	0.92	0.11	14.0	6.55	0.27	0.56	0.89	4.91	5.20	0.26	0.09	96.9
K09-618B	64.3	0.88	0.04	14.2	6.47	0.26	0.59	0.85	5.18	5.11	0.28	0.08	98.3
K09-618B	63.2	0.97	0.06	14.0	6.72	0.29	0.53	0.87	4.64	5.04	0.32	0.09	96.8
K09-618B	64.3	0.96	0.08	13.9	6.82	0.28	0.56	0.89	5.27	5.11	0.23	0.09	98.5
K09-618B	64.1	0.93	0.05	14.1	6.62	0.28	0.57	0.89	5.14	5.21	0.21	0.08	98.2
K09-618B	64.1	0.91	0.11	14.1	6.77	0.27	0.49	0.90	5.18	5.09	0.21	0.09	98.2
K09-618B	64.2	0.90	0.15	13.9	6.56	0.32	0.56	0.89	5.17	5.25	0.21	0.08	98.2
K09-618B	64.3	0.91	0.14	14.0	6.67	0.26	0.53	0.90	5.50	5.09	0.25	0.09	98.6
K09-618B	64.9	0.97	0.15	14.2	6.57	0.32	0.55	0.88	5.21	5.11	0.19	0.08	99.1
K09-618B	64.4	0.97	0.03	14.1	6.48	0.29	0.57	0.89	4.77	5.12	0.28	0.08	97.9
K09-618B	64.4	0.91	0.05	14.1	6.78	0.26	0.48	0.86	5.02	5.12	0.29	0.07	98.4
K09-618B	65.1	0.82	0.05	14.2	6.71	0.28	0.53	0.90	5.05	5.13	0.25	0.08	99.1
K09-618B	64.5	0.89	0.03	14.0	6.55	0.29	0.54	0.87	4.88	5.05	0.25	0.09	98.0
K09-618B	64.6	0.91	0.17	14.1	6.74	0.24	0.57	0.93	5.24	5.26	0.24	0.08	99.1
K09-618B	64.9	0.95	0.07	13.9	6.53	0.28	0.48	0.88	4.65	5.05	0.27	0.08	98.1
K09-618B	64.8	0.97	0.17	14.3	6.67	0.31	0.55	0.92	5.32	5.11	0.30	0.08	99.5
Average	**64.1**	**0.93**	**0.09**	**14.1**	**6.63**	**0.28**	**0.54**	**0.89**	**5.09**	**5.13**	**0.25**	**0.08**	**98.1**
s.d.	**0.9**	**0.04**	**0.05**	**0.2**	**0.11**	**0.02**	**0.03**	**0.02**	**0.23**	**0.08**	**0.04**	**0.01**	**0.9**

Individual analyses of feldspar from the Lower Kerichwa Tuff

Sample	SiO_2	Al_2O_3	Fe_2O_3	CaO	BaO	Na_2O	K_2O	Sum
K09-686	64.9	19.3	0.30	0.74	0.00	7.26	6.07	98.6
K09-686	64.9	19.2	0.40	0.42	0.07	7.15	6.44	98.7
K09-686	66.2	18.4	0.40	0.23	0.00	6.79	6.74	98.8
K09-686	65.1	19.7	0.29	1.08	0.00	8.16	4.39	98.8
K09-686	65.3	19.1	0.34	0.65	0.00	7.19	6.15	98.9
K09-686	66.0	18.6	0.41	0.16	0.00	6.84	6.80	98.9
K09-686	64.9	19.2	0.37	0.73	0.00	7.55	6.09	98.9
K09-686	65.8	18.9	0.32	0.24	0.00	7.21	6.69	99.1
K09-686	65.9	18.7	0.33	0.32	0.00	7.41	6.46	99.2
K09-686	66.3	18.7	0.49	0.18	0.00	6.86	7.03	99.5
K09-686	66.4	18.7	0.38	0.15	0.00	7.21	6.73	99.7
K09-686	66.4	18.6	0.47	0.14	0.00	7.43	6.59	99.7
K09-686	66.1	18.9	0.31	0.39	0.00	7.37	6.54	99.8
K09-686	66.4	18.5	0.43	0.17	0.00	7.37	6.83	99.8
K09-686	66.2	19.0	0.32	0.49	0.00	7.30	6.41	99.9
K09-686	66.8	18.7	0.43	0.14	0.00	7.36	6.64	100.1
K09-686	66.5	18.5	0.48	0.17	0.00	7.35	6.90	100.1
K09-686	66.8	19.0	0.42	0.33	0.01	7.20	6.74	100.5

SOM Table S4. U-Pb isotopic data for zircon crystals (samples KY13011903 and KY13012102, obtained from the fossiliferous bed) determined by LA-ICP-MS.

			Isotopic ratios							Concordance	Age (Ma)					Remarks
Mount ID	Spot ID	Ablation pit size (micron)	Th/ U	$^{207}Pb/^{206}Pb$	Error (2 □□□□	$^{206}Pb/^{238}U$	Error (2 □□□□	$^{207}Pb/^{235}U$	Error (2 □□□□		$^{206}Pb/^{238}U$	Error (2 □□□□)	$^{207}Pb/^{235}U$	Error (2 □□□□	U (ppm)	
KY13011903																
Tef.1	2	20	0.16	0.0763	0.0027	0.1043	0.00336	1.0759	0.088		639.5	21.6	741.6	85.6	136	
	3	20	0.01	0.0671	0.0024	0.10369	0.00325	0.9404	0.0696		636	20.9	673.1	68.4	240	
	5(1)	20	0.64	0.0728	0.0026	0.00059	0.00005	0.0058	0.0016	Discordant	3.8	0.3	5.9	1.6	513	youngest
	5(2)	25	-	0.4596	0.0176	0.00089	0.00007	0.0281	0.0026	Discordant	5.7	0.4	28.2	2.6	486	youngest
	5(3)	25	-	0.2797	0.0107	0.00057	0.00004	0.011	0.0012	Discordant	3.7	0.3	11.1	1.2	498	youngest
	6	20	0.36	0.0604	0.0021	0.10663	0.00383	0.8713	0.1044		653.1	24.7	636.3	100.8	43	
	7	20	0.14	0.0613	0.0028	0.10454	0.00335	0.8743	0.1136		640.9	21.5	637.9	109.2	34	
	8	20	0.45	0.0658	0.003	0.12144	0.00298	1.0905	0.0784		738.9	19.2	748.7	76.6	240	
	9(1)	20	1.11	0.0471	0.0022	0.00053	0.00003	0.0034	0.0008		3.4	0.2	3.4	0.8	1196	youngest
	9(2)	20	1.09	0.0509	0.0024	0.00051	0.00003	0.0036	0.0008		3.3	0.2	3.6	0.9	1151	youngest
	9(3)	25	-	0.1012	0.0039	0.00054	0.00004	0.0037	0.0006		3.5	0.3	3.8	0.6	448	youngest
	9(4)	25	-	0.2646	0.0101	0.00053	0.00007	0.0096	0.0023	Discordant	3.4	0.4	9.7	2.3	82	youngest
	10	20	0.06	0.062	0.0029	0.10034	0.00241	0.8494	0.0567		616.4	15.5	624.3	56	467	
	11(1)	20	0.42	0.0396	0.0018	0.00056	0.00009	0.003	0.0023		3.6	0.5	3.1	2.3	125	youngest
	11(2)	25	-	0.1153	0.0044	0.00055	0.00005	0.0044	0.0008		3.6	0.3	4.5	0.9	282	youngest
	12	20	0.16	0.0637	0.003	0.10429	0.00278	0.907	0.0812		639.5	17.9	655.5	79.3	99	
	13	20	0.15	0.0655	0.003	0.10181	0.00323	0.91	0.1146		625	20.8	657.1	110.2	36	
	14(1)	20	0.31	0.1548	0.0072	0.00087	0.00012	0.0184	0.0066	Discordant	5.6	0.8	18.5	6.7	93	

	14(2)	20	0.31	0.0167	0.0008	0.00178	0.00015	0.0041	0.0026		11.5	1	4.1	2.6	133	
Secondary standard (OD-3: ca. 33Ma)																
	OD3 2-4	25	-	0.0955	0.0037	0.00502	0.00033	0.033	0.0027		32.3	2.1	33	2.8	759	
	OD3 2-5	25	-	0.0949	0.0036	0.00514	0.00034	0.0336	0.0028		33	2.2	33.5	2.8	748	
	OD3 2-6	25	-	0.093	0.0036	0.0051	0.00034	0.0327	0.0027		32.8	2.2	32.7	2.7	763	
	OD3 2-7	25	-	0.0935	0.0036	0.00526	0.00036	0.0339	0.0036		33.8	2.3	33.8	3.7	198	
	OD3 2-8	25	-	0.1095	0.0042	0.00518	0.00035	0.039	0.0037		33.3	2.3	38.9	3.8	283	
KY13012102																
Tef.1	1	20	0.24	0.0583	0.0022	0.10574	0.00623	0.8302	0.1312		648	40	613.7	125.2	19	
	2	20	0.01	0.0603	0.0023	0.09895	0.00512	0.8043	0.039		608.3	32.9	599.2	38.8	252	
	3	20	0.17	0.0591	0.0022	0.10012	0.00542	0.7969	0.0778		615.1	34.9	595.1	76.1	52	
	4	20	0.27	0.0573	0.0022	0.10098	0.00579	0.7794	0.1097		620.2	37.2	585.1	105.7	25	
	5	20	0.18	0.0695	0.0026	0.10055	0.00562	0.9408	0.1096		617.6	36.1	673.3	105.6	33	
	6	20	0.19	0.0651	0.0025	0.09869	0.00596	0.8662	0.1438		606.7	38.3	633.5	136.4	17	
	7(1)	20	2.16	0.0328	0.0012	0.00099	0.00009	0.0044	0.0019		6.4	0.6	4.4	1.9	254	
	7(2)	20	2.27	0.0523	0.002	0.0011	0.0001	0.0077	0.0027		7.1	0.7	7.8	2.7	233	
	8	20	0.24	0.0703	0.0027	0.13967	0.0073	1.3231	0.0857		842.8	46.9	855.9	83.5	99	
	9	20	0.21	0.0616	0.0023	0.10382	0.00564	0.861	0.0857		636.7	36.2	630.7	83.5	48	
	10	20	0.28	0.061	0.0023	0.10276	0.00555	0.8446	0.0801		630.6	35.7	621.7	78.2	54	
	11	20	0.1	0.0613	0.0023	0.10586	0.00552	0.8736	0.0533		648.7	35.5	637.5	52.7	139	
	12	20	0.3	0.185	0.007	0.50375	0.02633	12.5564	1.0301		2629.9	167.5	2647	719	36	
	13(1)	20	1.32	0.0801	0.003	0.00055	0.00004	0.0059	0.0012	Discordance	3.5	0.3	6	1.2	939	youngest
	13(2)	25	-	0.0928	0.0018	0.00055	0.00002	0.0035	0.0004		3.6	0.1	3.6	0.4	1136	youngest
	13(3)	25	-	0.1006	0.0039	0.00051	0.00004	0.0035	0.0004		3.3	0.2	3.6	0.4	1106	youngest

	14	20	0.23	0.0626	0.0021	0.10367	0.00433	0.8652	0.0918		635.9	27.8	632.9	89.2	43	
	15	20	0.27	0.0712	0.0024	0.10451	0.00478	0.9917	0.138		640.8	30.7	699.6	131.2	23	
	16	20	0.2	0.063	0.0021	0.10398	0.00417	0.8735	0.0765		637.7	26.8	637.5	74.9	64	
	17(1)	20	0.81	0.1203	0.0041	0.00113	0.00026	0.0181	0.0119		7.3	1.7	18.2	12	28	
	17(2)	20	0.82	0.2563	0.0087	0.0008	0.00022	0.0274	0.0146	Discordance	5.2	1.4	27.5	14.8	28	
	18	20	0.22	0.0613	0.0021	0.10161	0.00414	0.8304	0.0796		623.9	26.7	613.8	77.8	54	
	19	20	0.25	0.0614	0.0021	0.10428	0.00398	0.8532	0.0519		639.4	25.6	626.4	51.3	147	
	20	20	0.22	0.0673	0.0023	0.09833	0.00409	0.8814	0.0901		604.6	26.3	641.8	87.6	46	
Tef.2	1	25	-	0.1282	0.0053	0.09848	0.00348	0.8521	0.0292		605.5	22.4	625.8	29.2	257	
	2	25	-	0.1238	0.0052	0.10527	0.00396	0.8794	0.0582		645.2	25.5	640.7	57.4	33	
	3(1)	25	-	0.044	0.0018	0.00062	0.00008	0.0018	0.001		4	0.5	1.9	1	72	youngest
	3(2)	25	-	-0.0086	-0.0003	0.00059	0.00008	-0.0004	#NUM!	Discordance	3.8	0.5	-0.4	#NUM!	72	youngest
	3(3)	25	-	0.0275	0.0011	0.00056	0.00008	0.0011	0.0008		3.6	0.5	1.1	0.8	70	youngest
	4	25	-	0.1221	0.0051	0.1069	0.00382	0.8809	0.0363		654.7	24.6	641.4	36.2	122	
	5	25	-	0.1378	0.0057	0.14825	0.00527	1.3787	0.0544		891.2	33.9	879.9	53.8	122	
	6	25	-	0.124	0.0052	0.10524	0.00392	0.8807	0.0541		645.1	25.2	641.4	53.5	40	
	7	25	-	0.0838	0.0035	0.00095	0.00007	0.0054	0.0012		6.1	0.5	5.4	1.2	152	
	8	25	-	0.1224	0.0051	0.10347	0.00378	0.8549	0.0446		634.7	24.3	627.3	44.3	61	
	10	25	-	0.1233	0.0051	0.09908	0.00372	0.8245	0.0529		609	23.9	610.5	52.3	37	
	11	25	-	0.324	0.0135	0.38629	0.01392	8.4465	0.4968		2105.6	89.1	2280.2	409.6	29	
	12	25	-	0.1235	0.0051	0.10187	0.00375	0.8488	0.0479		625.3	24.1	624	47.5	50	
	13	25	-	0.123	0.0049	0.10357	0.00365	0.8613	0.0684		635.3	23.5	630.8	67.2	22	
	14	25	-	0.1252	0.005	0.10719	0.00357	0.9077	0.056		656.4	22.9	655.9	55.3	39	
	15	25	-	0.1358	0.0054	0.13548	0.00431	1.2438	0.0566		819.1	27.7	820.6	55.9	82	

16	25	-	0.1363	0.0055	0.31601	0.0098	2.9136	0.0989		1770.2	62.8	1385.5	95.7	230	
17(1)	25	-	0.1347	0.0054	0.00058	0.00005	0.0053	0.0012	Discordance	3.8	0.3	5.4	1.2	150	youngest
17(2)	25	-	0.0962	0.0037	0.00058	0.00007	0.0039	0.0012		3.8	0.4	3.9	1.2	116	youngest
17(3)	25	-	0.1297	0.005	0.00061	0.00007	0.0055	0.0016		3.9	0.5	5.5	1.6	91	youngest
18	25	-	0.136	0.0054	0.1395	0.00439	1.2834	0.0525		841.8	28.3	838.4	51.9	117	
19	25	-	0.1224	0.0049	0.10559	0.0034	0.8743	0.0431		647.1	21.9	637.9	42.9	73	
20	25	-	0.0938	0.0038	0.00051	0.00003	0.0032	0.0005		3.3	0.2	3.3	0.5	618	youngest
21	25	-	0.1238	0.0050	0.10460	0.00343	0.8759	0.0498		641.3	22.1	638.7	49.3	49	
22(1)	25	-	0.2478	0.0099	0.00068	0.00006	0.0114	0.0020	Discordance	4.4	0.4	11.5	2.0	124	
22(2)	25	-	0.0024	0.0001	0.00278	0.00023	0.0005	0.0005		17.9	1.5	0.5	0.5	75	
23(1)	25	-	0.0445	0.0018	0.00050	0.00005	0.0015	0.0007		3.2	0.3	1.5	0.7	118	youngest
23(2)	25	-	0.4766	0.0183	0.00077	0.00009	0.0252	0.0039	Discordance	4.9	0.6	25.2	3.9	89	youngest
23(3)	25	-	0.6867	0.0263	0.00082	0.00009	0.0388	0.0053	Discordance	5.3	0.6	38.7	5.4	82	youngest
23(4)	25	-	0.6385	0.0245	0.00099	0.00011	0.0434	0.0057	Discordance	6.4	0.7	43.1	5.8	81	youngest
24	25	-	0.1359	0.0054	0.14092	0.00449	1.2956	0.0603		849.9	28.9	843.8	59.5	76	
29	25	-	0.1370	0.0055	0.15181	0.00481	1.4069	0.0635		911.1	31.0	891.8	62.5	82	
Secondary standard (OD-3: ca.33Ma)															
OD3 1-1	25	-	0.1103	0.0046	0.00512	0.00022	0.0381	0.0029	Discordance	32.9	1.4	38.0	3.0	222	
OD3 1-2	25	-	0.0930	0.0039	0.00509	0.00026	0.0319	0.0042		32.7	1.7	31.9	4.2	83	
OD3 1-3	25	-	0.0972	0.0041	0.00520	0.00022	0.0342	0.0029		33.5	1.4	34.1	2.9	202	
OD3 2-1	25	-	0.0783	0.0031	0.00511	0.00025	0.0271	0.0038		32.9	1.6	27.1	3.8	84	
OD3 2-2	25	-	0.0956	0.0037	0.00489	0.00033	0.0322	0.0029		31.5	2.1	32.2	2.9	487	
OD3 2-3	25	-	0.0946	0.0036	0.00493	0.00032	0.0321	0.0025		31.7	2.1	32.1	2.6	1297	

SOM Table S6. Isotopic analyses of enamel from fossil mammals at the Kantis Fossil Site. (a) KFS individual data and (b) statistics of KFS, Lothagam (Kaiyumung Mb; 3.2 Ma), Laetoli (Upper Laetoli Beds; 3.8-3.5 Ma), Dikika (Sidi Hakoma Mb; 3.4 Ma) and Koobi Fora (Lokochot Mb; 3.5 Ma).

Accession number KNM-RK	Order	Family	Species	$\delta^{13}C$ (‰)
50004	Artiodactyla	Hippopotamidae	aff. *Hippopotamus* cf. *protamphibius*	-0.73
50005			aff. *Hippopotamus* cf. *protamphibius*	-0.19
50023			aff. *Hippopotamus* cf. *protamphibius*	-3.47
50035			aff. *Hippopotamus* cf. *protamphibius*	0.38
50037			aff. *Hippopotamus* cf. *protamphibius*	-4.50
50042			aff. *Hippopotamus* cf. *protamphibius*	-1.47
50058			aff. *Hippopotamus* cf. *protamphibius*	-2.43
50065			aff. *Hippopotamus* cf. *protamphibius*	0.26
50554			aff. *Hippopotamus* cf. *protamphibius*	-0.69
50591			aff. *Hippopotamus* cf. *protamphibius*	-0.58
50613			aff. *Hippopotamus* cf. *protamphibius*	-3.37
51174			aff. *Hippopotamus* cf. *protamphibius*	-2.77
51215			aff. *Hippopotamus* cf. *protamphibius*	-3.46
51225			aff. *Hippopotamus* cf. *protamphibius*	-0.96
51226			aff. *Hippopotamus* cf. *protamphibius*	-4.72
51378			aff. *Hippopotamus* cf. *protamphibius*	-3.37
51381			aff. *Hippopotamus* cf. *protamphibius*	-1.03
55276			aff. *Hippopotamus* cf. *protamphibius*	-1.65
55277			aff. *Hippopotamus* cf. *protamphibius*	-5.70
55280			aff. *Hippopotamus* cf. *protamphibius*	-0.93
55275			aff. *Hippopotamus* cf. *protamphibius*	-0.92
55282			aff. *Hippopotamus* cf. *protamphibius*	-2.09
55283			aff. *Hippopotamus* cf. *protamphibius*	-1.59
55284			aff. *Hippopotamus* cf. *protamphibius*	-5.32
55285			aff. *Hippopotamus* cf. *protamphibius*	-2.03
55286			aff. *Hippopotamus* cf. *protamphibius*	-1.88
55287			aff. *Hippopotamus* cf. *protamphibius*	-1.09
55288			aff. *Hippopotamus* cf. *protamphibius*	-1.58
55290			aff. *Hippopotamus* cf. *protamphibius*	-5.78
55432			aff. *Hippopotamus* cf. *protamphibius*	-2.70
48738	Artiodactyla	Bovidae	Alcelaphini	-4.32
48746			Alcelaphini	-10.33
48750			Bovini	-0.59
50002			*Aepyceros*	-4.03
50062			(probably) Bovini	1.61
50066			Alcelaphini or *Aepyceros*	0.34
50458			Alcelaphini	-4.10
50476			Alcelaphini	-3.81
50503			Bovini	0.44
50518			Alcelaphini	-2.55

50628			*Aepyceros*	-6.87
51159			Alcelaphini	-5.54
51196			Bovini	-4.22
48744	Artiodactyla	Suidae	*Notochoerus* cf. *euilus*	-1.12
48749			*Notochoerus* cf. *euilus*	-0.77
50051			*Notochoerus* cf. *euilus*	-0.84
50069			*Notochoerus* cf. *euilus*	-0.45
50494			*Notochoerus* cf. *euilus*	-0.99
50539			*Notochoerus* cf. *euilus*	-0.23
50621			*Notochoerus* cf. *euilus*	-1.78
54221			*Notochoerus* cf. *euilus*	-2.08
54226			*Notochoerus* cf. *euilus*	-0.39
54220			*Notochoerus* cf. *euilus*	-1.34
52994			*Notochoerus* cf. *euilus*	-0.94
54224			*Notochoerus* cf. *euilus*	-1.71
54223			*Notochoerus* cf. *euilus*	-0.98
54222			*Notochoerus* cf. *euilus*	0.02
55266			*Notochoerus* cf. *euilus*	-1.03
55435			*Notochoerus* cf. *euilus*	-1.05
55637			*Notochoerus* cf. *euilus*	-0.03
55642			*Notochoerus* cf. *euilus*	-1.30
55648			*Notochoerus* cf. *euilus*	-0.30
55684			*Notochoerus* cf. *euilus*	-0.69
55650			*Notochoerus* cf. *euilus*	-0.59
55641			*Notochoerus* cf. *euilus*	-0.40
52981	Artiodactyla	Giraffidae	*Sivatherium*	-11.16
50499			*Sivatherium*	-10.69
50534			*Sivatherium*	-10.79
55335			*Sivatherium*	-11.09
56128			*Sivatherium*	-14.04
49989	Perissodactyla	Rhinocerotidae	*Ceratotherium mauritanicum*	-2.83
50000			*Ceratotherium mauritanicum*	-3.21
50585			*Ceratotherium mauritanicum*	-4.45
50601			*Ceratotherium mauritanicum*	-4.81
50692			*Ceratotherium mauritanicum*	-4.94
51220			*Ceratotherium mauritanicum*	-5.35
51274			*Ceratotherium mauritanicum*	-4.56
56109			*Ceratotherium mauritanicum*	-7.33
56108			*Ceratotherium mauritanicum*	-5.40
56115			*Ceratotherium mauritanicum*	-4.42
56114			*Ceratotherium mauritanicum*	-4.84
56112			*Ceratotherium mauritanicum*	-6.14
56110			*Ceratotherium mauritanicum*	-8.07
56113			*Ceratotherium mauritanicum*	-6.92
56111			*Ceratotherium mauritanicum*	-6.07
55339			*Diceros sp.*	-5.61
53790			*Ceratotherium mauritanicum*	-5.65

53810			*Ceratotherium mauritanicum*	-4.71
53798			*Ceratotherium mauritanicum*	-4.04
53806			*Ceratotherium mauritanicum*	-3.85
53809			*Ceratotherium mauritanicum*	-5.02
53807			*Ceratotherium mauritanicum*	-4.85
53808			*Ceratotherium mauritanicum*	-4.50
52979			*Ceratotherium mauritanicum*	-6.70
52980			*Ceratotherium mauritanicum*	-5.93
53540			*Ceratotherium mauritanicum*	-4.36
49993	Perissodactyla	Equidae	*Hipparion sp.*	-0.37
50034			*Hipparion sp.*	0.15
50526			*Hipparion sp.*	-3.86
51238			*Hipparion sp.*	-1.21
51270			*Hipparion sp.*	-0.88
51390			*Hipparion sp.*	0.00
55350			*Hipparion sp.*	0.22
55351			*Hipparion sp.*	-0.47
55352			*Hipparion sp.*	-0.81
55356			*Hipparion sp.*	0.31
55500			*Hipparion sp.*	-0.53
56119			*Hipparion sp.*	-2.32
56118			*Hipparion sp.*	-0.99
56117			*Hipparion sp.*	-0.35
56116			*Hipparion sp.*	0.77
52988	Proboscidea	Elephantidae	*indet*	-1.28
48735			*indet*	-3.26
56120			*indet*	-3.37
56127			*indet*	-2.25
57541			*indet*	-2.17